nated site because the intensity of the peak for the deaminated product CCUA (peak 4) was greater than that of the peak corresponding to CCUU (peak 3). A3G would exploit this sequential preference to efficiently deaminate multiple hot spots that are scattered throughout the HIV genome with a small amount of redundant deamination of CCCC.

In conclusion, we analyzed real-time NMR data for the location-dependent deamination by A3G CD2 using a newly derived kinetic model. As a result, the location-dependent deamination can be explained by the difference in the rate constants k_{cat} of CD2, which depend on the direction of the approach to the target cytidine. We also characterized deamination reactions of CCCC by real-time NMR spectroscopy, even though multiple reactions occurred simultaneously. Previously, it was proposed that the location-dependent deamination is caused by two binding orientations on ssDNA and the existence of a region where either less or no deamination occurs (ca. 30 nucleotides) at the 3′ end of the ssDNA.[10,16] However, this model cannot explain the location-dependent deamination that is observed for long ssDNA (70 nucleotides)[15] because the contribution of the dead region to the location dependency becomes smaller. On the other hand, our model can explain the location-dependent deamination reaction even for such a long ssDNA fragment.

Recently, it was proposed that the proteins of the APOBEC family are involved in epigenesis.[22] They may contribute to the removal of an epigenetic marker, a methyl group of a 5-methyl cytosine, through deamination of 5-hydroxymethyl cytosine. Our real-time NMR method could also be applied to examine such DNA modifications and to provide insight into epigenesis. Furthermore, this method can also be used for the analysis of post-translation modifications of proteins.

Received: November 15, 2013
Published online: January 29, 2014

Keywords: deamination · DNA · enzyme kinetics · quantitative analysis · NMR spectroscopy

[1] A. M. Sheehy, N. C. Gaddis, J. D. Choi, M. H. Malim, *Nature* **2002**, *418*, 646–650.
[2] R. S. Harris, M. T. Liddament, *Nat. Rev. Immunol.* **2004**, *4*, 868–877.
[3] D. Lecossier, F. Bouchonnet, F. Clavel, A. J. Hance, *Science* **2003**, *300*, 1112.
[4] B. Mangeat, P. Turelli, G. Caron, M. Friedli, L. Perrin, D. Trono, *Nature* **2003**, *424*, 99–103.
[5] H. Zhang, B. Yang, R. J. Pomerantz, C. Zhang, S. C. Arunachalam, L. Gao, *Nature* **2003**, *424*, 94–98.
[6] R. S. Harris, K. N. Bishop, A. M. Sheehy, H. M. Craig, S. K. Petersen-Mahrt, I. N. Watt, M. S. Neuberger, M. H. Malim, *Cell* **2003**, *113*, 803–809.
[7] G. Hache, M. T. Liddament, R. S. Harris, *J. Biol. Chem.* **2005**, *280*, 10920–10924.
[8] F. Navarro, B. Bollman, H. Chen, R. Konig, Q. Yu, K. Chiles, N. R. Landau, *Virology* **2005**, *333*, 374–386.
[9] Q. Yu, R. Konig, S. Pillai, K. Chiles, M. Kearney, S. Palmer, D. Richman, J. M. Coffin, N. R. Landau, *Nat. Struct. Mol. Biol.* **2004**, *11*, 435–442.
[10] L. Chelico, P. Pham, P. Calabrese, M. F. Goodman, *Nat. Struct. Mol. Biol.* **2006**, *13*, 392–399.
[11] L. S. Shlyakhtenko, A. Y. Lushnikov, A. Miyagi, M. Li, R. S. Harris, Y. L. Lyubchenko, *Biochemistry* **2012**, *51*, 6432–6440.
[12] G. Senavirathne, M. Jaszczur, P. A. Auerbach, T. G. Upton, L. Chelico, M. F. Goodman, D. Rueda, *J. Biol. Chem.* **2012**, *287*, 15826–15835.
[13] R. Suspène, C. Rusniok, J. P. Vartanian, S. Wain-Hobson, *Nucleic Acids Res.* **2006**, *34*, 4677–4684.
[14] L. G. Holden, C. Prochnow, Y. P. Chang, R. Bransteitter, L. Chelico, U. Sen, R. C. Stevens, M. F. Goodman, X. S. Chen, *Nature* **2008**, *456*, 121–124.
[15] R. Nowarski, E. Britan-Rosich, T. Shiloach, M. Kotler, *Nat. Struct. Mol. Biol.* **2008**, *15*, 1059–1066.
[16] L. Chelico, C. Prochnow, D. A. Erie, X. S. Chen, M. F. Goodman, *J. Biol. Chem.* **2010**, *285*, 16195–16205.
[17] A. Furukawa, T. Nagata, A. Matsugami, Y. Habu, R. Sugiyama, F. Hayashi, N. Kobayashi, S. Yokoyama, H. Takaku, M. Katahira, *EMBO J.* **2009**, *28*, 440–451.
[18] S. Harjes, W. C. Solomon, M. Li, K. M. Chen, E. Harjes, R. S. Harris, H. Matsuo, *J. Virol.* **2013**, *87*, 7008–7014.
[19] I. J. Byeon, J. Ahn, M. Mitra, C. H. Byeon, K. Hercik, J. Hritz, L. M. Charlton, J. G. Levin, A. M. Gronenborn, *Nat. Commun.* **2013**, *4*, 1890.
[20] K. M. Chen, E. Harjes, P. J. Gross, A. Fahmy, Y. Lu, K. Shindo, R. S. Harris, H. Matsuo, *Nature* **2008**, *452*, 116–119.
[21] K. Sugase, T. Konuma, J. C. Lansing, P. E. Wright, *J. Biomol. NMR* **2013**, *56*, 275–283.
[22] N. Bhutani, D. M. Burns, H. M. Blau, *Cell* **2011**, *146*, 866–872.

EUROPEAN JOURNAL OF Haematology

European Journal of Haematology 92 (219–228)

ORIGINAL ARTICLE

Antitumor effects of bevacizumab in a microenvironment-dependent human adult T-cell leukemia/lymphoma mouse model

Fumiko Mori[1], Takashi Ishida[1], Asahi Ito[1], Fumihiko Sato[2], Ayako Masaki[1], Tomoko Narita[1], Susumu Suzuki[2], Tomiko Yamada[1], Hisashi Takino[2], Masaki Ri[1], Shigeru Kusumoto[1], Hirokazu Komatsu[1], Masakatsu Hishizawa[3], Kazunori Imada[4], Akifumi Takaori-Kondo[3], Akio Niimi[1], Ryuzo Ueda[5], Hiroshi Inagaki[2], Shinsuke Iida[1]

[1]Department of Medical Oncology and Immunology, Nagoya City University Graduate School of Medical Sciences, Nagoya;[2]Department of Anatomic Pathology and Molecular Diagnostics, Nagoya City University Graduate School of Medical Sciences, Nagoya; [3]Department of Hematology and Oncology, Graduate School of Medicine, Kyoto University, Kyoto; [4]Department of Hematology, Kokura Memorial Hospital, Kitakyushu; [5]Department of Tumor Immunology, Aichi Medical University School of Medicine, Nagakute, Japan

Abstract

Objective: The objective of this study was to evaluate the therapeutic potential of bevacizumab with or without systemic chemotherapy for adult T-cell leukemia/lymphoma (ATL) and clarify the significance of angiogenesis for ATL pathogenesis. *Methods:* NOD/Shi-*scid*, IL-2Rγ^{null} (NOG) mice were used as recipients of tumor cells from a patient with ATL, which engraft and proliferate in a microenvironment-dependent manner. The ATL cells could be serially transplanted in NOG mice, but could not be maintained in *in vitro* cultures. *Results:* Injection of bevacizumab alone significantly increased necrosis and decreased vascularization in the tumor tissue. Levels of human soluble interleukin two receptor in the serum (reflecting the ATL tumor burden) of bevacizumab-treated mice were significantly lower than in untreated mice. Although bevacizumab monotherapy showed these clear anti-angiogenesis effects, it did not prolong survival. In contrast, injection of bevacizumab together with cyclophosphamide, doxorubicin, vincristine, prednisolone (CHOP) led to a significant prolongation of survival of the ATL mice relative to CHOP alone. *Conclusions:* This is the first report to evaluate the efficacy of bevacizumab for ATL in a tumor microenvironment-dependent model. Bevacizumab therapy combined with chemotherapy could be a valuable treatment strategy for that subgroup of ATL probably depending to a large extent on angiogenesis via vascular endothelial growth factor.

Key words Adult T-cell leukemia-lymphoma; Bevacizumab; tumor microenvironment

Correspondence Takashi Ishida, MD, PhD, Department of Medical Oncology and Immunology, Nagoya City University Graduate School of Medical Sciences, 1 Kawasumi, Mizuho-chou, Mizuho-ku, Nagoya, Aichi 467-8601, Japan. Tel: +81 52 853 8216; Fax: +81 52 852 0849; e-mail: itakashi@med.nagoya-cu.ac.jp

Accepted for publication 29 October 2013

doi:10.1111/ejh.12231

Adult T-cell leukemia-lymphoma (ATL) is an aggressive peripheral T-cell neoplasm caused by human T-cell lymphotropic virus type 1 (HTLV-1). The disease is resistant to conventional chemotherapeutic agents, and currently there are only limited treatment options; thus, it has a very poor prognosis (1–4). Over the past decade, allogeneic hematopoietic stem-cell transplantation has evolved into a potential approach to treating patients with ATL. However, only a small fraction of patients have the opportunity to benefit from transplantation, such as those who are younger, have achieved sufficient disease control, and have an appropriate stem-cell source (5, 6). Therefore, the development of alternative treatment strategies for patients with ATL is an urgent issue.

Bevacizumab is a humanized monoclonal antibody against the vascular endothelial growth factor A (VEGF-A), a key

factor inducing the formation of blood vessels (angiogenesis) in tumors (7). Bevacizumab is currently approved worldwide for the treatment of several types of cancer such as metastatic colorectal cancer, metastatic non-small-cell lung cancer, renal cell carcinoma, and advanced ovarian cancer, in combination with chemotherapy or interferon (8–14). Bevacizumab is also approved as a single agent for recurrent glioblastoma in the USA (15). In this context, many aspects of pathological angiogenesis have been extensively studied in many types of cancer. On the other hand, the precise role of these processes in pathogenesis of hematological malignancies including ATL is still under active investigation (16–19). Thus far, bevacizumab has not been approved for the treatment of any hematological malignancy in the USA, Europe, or Japan. The aim of the present study was to evaluate the therapeutic potential of bevacizumab with or without systemic chemotherapy for ATL and clarify the significance of angiogenesis for ATL pathogenesis, using a microenvironment-dependent murine ATL model.

Methods

Animals

NOD/Shi-*scid*, IL-2Rγ^{null} (NOG) mice (20) were purchased from the Central Institute for Experimental Animals (Kanagawa, Japan) and used at 6–8 wk of age. All of the *in vivo* experiments were performed in accordance with the United Kingdom Coordinating Committee on Cancer Research Guidelines for the Welfare of Animals in Experimental Neoplasia, Second Edition, and were approved by the Ethics Committee of the Center for Experimental Animal Science, Nagoya City University Graduate School of Medical Sciences.

Immunopathological analysis

We assessed the affected lymph nodes of 23 patients with ATL by immunopathology. The patients provided written informed consent in accordance with the Declaration of Helsinki, and this present study was approved by the institutional Ethics Committee of Nagoya City University Graduate School of Medical Sciences. Hematoxylin and eosin (HE) staining and immunostaining using anti-human CD4 (4B12; Novocastra, Wetzlar, Germany), CD25 (4C9; Novocastra), CD20 (L26; DAKO, Glostrup, Denmark), VEGF-A (sc-152, rabbit polyclonal; Santa Cruz, Heidelberg, Germany), Alpha-Smooth Muscle Actin (α-SMA) (1A4; DAKO), CD31 (JC70A; DAKO), and von Willebrand Factor (Rabbit polyclonal; DAKO) were performed on formalin-fixed, paraffin-embedded sections. VEGF-A expression levels were categorized according to the following formula: 3+ positive if ≥50%, 2+ positive if <50 ≥30%, 1+ positive if <30 ≥10%, and negative if <10% of the ATL tumor cells were stained with the corresponding antibody. Nine 100× high-power fields (HPF) of HE tumor specimens were randomly selected, and the area of tumor necrosis (%) was calculated by Image J software (21), and then averaged. Nine 100× HPF of von Willebrand Factor-stained tumor specimens were randomly selected, and numbers of vessels (per mm^2) were calculated by Image J software and then averaged.

ATL mouse model

A leukemic cell clone from a patient with ATL, which could be serially transplanted into SCID mice, designated S-YU as reported previously (22), was injected intraperitoneally (i.p.) into NOG mice. Three to 4 wk after i.p. injection, NOG mice were presented with intraperitoneal masses along the mesentery. Cells from these intraperitoneal masses were suspended in RPMI-1640 and inoculated i.p. into healthy NOG mice, which then presented with features identical to those of the original mice.

Cell lines

ATN-1, MT-1, and TL-Om1 are ATL cell lines, whereas MT-2, MT-4, and TL-Su are HTLV-1-immortalized lines, as previously described (23).

Quantitative reverse transcription-polymerase chain reaction

Total RNA was isolated with RNeasy Mini Kits (QIAGEN, Tokyo, Japan). Reverse transcription from the RNA to first strand cDNA was carried out using High Capacity RNA-to-cDNA Kits (Applied Biosystems Inc, Foster City, CA, USA). *Human VEGF-A* (Hs00900055_m1), *VEGF-R1* (Hs00176573_m1), *VEGF-R2* (Hs00911700_m1), and *β-actin* (Hs99999903_m1) *mRNA* were amplified using TaqMan® Gene Expression Assays with the aid of an Applied Biosystems StepOnePlus™. The quantitative assessment of the mRNA of interest was done by dividing its level by that of *β-actin* and expressing the result relative to Human Testis Total RNA (Clontech, Mountain View, CA, USA) as 1.0. All expressed values were averages of triplicate experiments.

Monoclonal antibodies and flow cytometry

The following Monoclonal antibodies (mAbs) were used for flow cytometry: APC-conjugated anti-human CD45 mAb (2D1; BD Biosciences, San Jose, CA, USA), PerCP-conjugated anti-CD4 mAb (SK3; BD Biosciences), PE-conjugated anti-CD25 mAb (M-A251; BD Biosciences), PE-conjugated VEGF-R1 mAb (49560; BD Biosciences), PE-conjugated VEGF-R2 mAb (89106, R&D Systems, Inc. Minneapolis, MN,

USA), and the appropriate isotype control mAbs. Whole blood was treated with BD FACS lysing solution (BD Biosciences) to remove RBC. Stained cells were analyzed on a FACSCalibur (BD Biosciences) with the aid of FlowJo software (Tree Star, Inc. Ashland, OR, USA).

Cell proliferation assay

Proliferation of S-YU and HTLV-I-immortalized lines expressing both VEGF-A and VEGF-R1 in the presence of different concentrations of bevacizumab for 48 h was assessed using CellTiter 96 Aqueous One Solution cell proliferation assay kits (Promega Corporation, Madison, WI, USA). Bevacizumab was purchased from Chugai Pharmaceutical Co., Ltd., Tokyo, Japan.

ATL cell-bearing mice treated with bevacizumab

ATL tumor cells (S-YU) from the intraperitoneal masses were suspended in RPMI-1640, and 1.0×10^7 was inoculated i.p. into each of 14 NOG mice. The animals were divided into two groups of seven each for treatment with bevacizumab or to serve as controls. Bevacizumab (10 mg/kg) or vehicle (saline) was i.p. injected into the mice 3, 10, and 17 d after tumor cell inoculations. Therapeutic efficacies were evaluated for area of tumor necrosis, number of vessels, and serum human sIL2R levels 22 d after tumor inoculation. The concentration of human sIL2R in the serum was measured by ELISA using human sIL2R immunoassay kits (R&D Systems, Inc.).

ATL cells from the intraperitoneal masses suspended in RPMI-1640 were also inoculated i.p. into another 10 NOG mice at 1.0×10^7 per mouse. These animals were randomly divided into two groups of five each for treatment with bevacizumab or as controls. Bevacizumab (10 mg/kg) or saline was injected i.p. into the mice 2, 9, 16, and 23 d after tumor cell inoculation. Therapeutic efficacy of bevacizumab was evaluated by survival times.

A further 16 NOG mice that had also received 1.0×10^7 ATL cells from intraperitoneal masses were randomly divided into two groups of eight each for treatment with bevacizumab + cyclophosphamide, doxorubicin, vincristine, prednisolone (CHOP) or CHOP alone. Bevacizumab (10 mg/kg) or saline was i.p. injected into the mice 2, 9, 16, 23, 30, and 37 d after tumor cell inoculations. CHOP was given i.p. 17 d after tumor inoculation at the following doses: cyclophosphamide, 40 mg/kg; doxorubicin, 3.3 mg/kg; vincristine, 0.5 mg/kg; and prednisolone, 0.2 mg/kg (24, 25). Therapeutic efficacy of bevacizumab was evaluated by survival time. Cyclophosphamide and vincristine were purchased from Shionogi Pharmaceutical Co., Ltd, Osaka, Japan; doxorubicin was from Kyowa Hakko Kirin Co., Ltd, Tokyo, Japan, and prednisolone was from Nippon Kayaku Co., Ltd, Tokyo, Japan.

Statistical analysis

The differences between groups regarding the tumor necrosis area, vascular number, and human sIL2R concentrations in serum were analyzed by the Mann–Whitney U test. In this study, $P < 0.05$ was considered significant.

Results

VEGF-A expression in ATL

VEGF-A expression by ATL cells in the lymph node lesions is shown in Fig. 1A. Immunopathological features of four cases from each group stratified by VEGF-A expression are shown in Fig. 1B. Most of the ATL cases (96%) were positive for VEGF-A.

ATL cell-bearing NOG mice

In earlier studies, S-YU ATL tumor cells, which were serially transplanted into SCID mice (22), manifested multiple enlarged mesenteric lymph nodes. In the present study, in which NOG mice rather than SCID mice were the S-YU recipients, larger tumor masses formed along the intestinal tract. Figure 2A shows the intraperitoneal masses and intestinal tract adhering tightly to one another in a NOG mouse (demarcated by thin white dotted lines in the figure). Flow cytometric analysis demonstrated that the mass mainly consisted of human cells expressing CD4 and CD25 (Fig. 2B). Immunopathological analysis revealed large atypical cells with irregular and pleomorphic nuclei, and blood vessels. The cells were CD4-positive, CD25-positive, but CD20-negative (Fig. 2C). These findings are consistent with an ATL cell phenotype in humans, and with earlier studies in the SCID/S-YU model. The S-YU tumor cells in the NOG mice were classed as VEGF-A 1+ positive (Fig. 2C). Blood vessels in the tumor tissue were stained by anti-α-SMA Ab (Fig. 2C). Vascular endothelial cells in the tumor tissue were stained by anti-von Willebrand Factor Ab, but not by anti-CD31 mAb (data not shown). Together, these results show that the blood vessels in the tumor tissue originated from the mouse, because anti-α-SMA and von Willebrand Factor Ab used in this study recognized the corresponding protein derived from both human and mouse, whereas the anti-CD31 mAb recognized the corresponding human but not murine protein (data not shown). CD4-positive CD25-positive ATL cell mild infiltration into spleen, liver, and bone marrow was seen by flow cytometry (Fig. 2D).

VEGF-A, VEGF-R1, and -R2 expression in ATL and HTLV-1-immortalized lines

VEGF-A mRNA expression was detected in all 7 ATL and HTLV-1-immortalized lines tested, and in S-YU cells

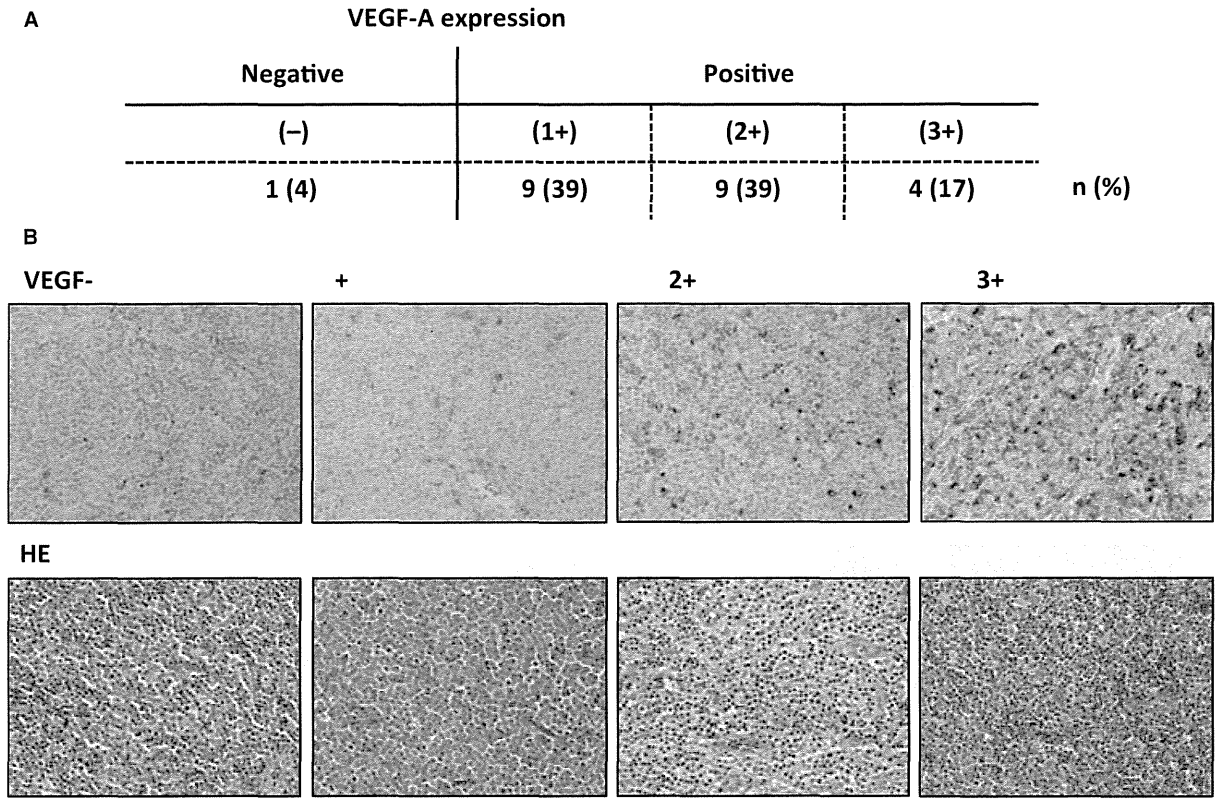

Figure 1 Vascular endothelial growth factor A (VEGF-A) expression in ATL. (A) VEGF-A expression of ATL cells in the lymph node lesion. VEGF-A expression was categorized based on the percentage of ATL cells stained as follows: ≥50%, 3+ positive; 30–49%, 2+ positive; 10–29%, 1+ positive; <10%, negative. (B) Cases 1, 2, 3, and 4 are representative of VEGF-A-negative, 1+, 2+, and 3+ positive categories, respectively. Photomicrographs with VEGF-A (upper panels) and hematoxylin and eosin staining (lower panels) are shown.

from intraperitoneal masses (Fig. 3A, upper left panel). *VEGF-R1 mRNA* expression was not present in ATL and in only two HTLV-1-immortalized lines (MT-2 and TL-Su) but was present in S-YU cells (Fig. 3A, upper right panel). No *VEGF-R2 mRNA* expression was detected in any of the 7 ATL and HTLV-1-immortalized lines tested, or in S-YU cells (data not shown). Flow cytometry demonstrated that VEGF-R1 protein was also expressed in MT-2 and TL-Su, and very weakly in NOG S-YU cells (Fig. 3A, lower panels), consistent with the RT-PCR results. Flow cytometry demonstrated that VEGF-R2 was not expressed at all in any of the ATL and HTLV-1-immortalized lines tested, or in S-YU cells (data not shown), which was also consistent with the RT-PCR results.

VEGF-R1 and VEGF-R2 expression in primary ATL cells

CD4-positive CD25-positive primary ATL cells in PBMC obtained from nine individual patients with ATL (i–ix) were evaluated for VEGF-R1 and -R2 expression. VEGF-R1 protein was expressed in only one patient (patient v) and VEGF-R2 was not expressed in any of the patients (Fig. 4B).

No Bevacizumab-mediated anti-proliferative activity against HTLV-1-immortalized lines and S-YU *in vitro*

Bevacizumab did not directly block the proliferation of MT-2 and TL-Su cells *in vitro*, despite their expression of both VEGF-A and VEGF-R1. Neither did it inhibit S-YU cells (Fig. 3C).

Therapeutic efficacy of bevacizumab monotherapy in S-YU cell-bearing NOG mice

Photomicrographs of tumor tissue from each mouse are shown (Fig. 4A). Treatment with bevacizumab resulted in an increased percentage of tumor necrosis in the NOG/S-YU mice (mean 25.3%, median 24.1%, range 19.2–33.6%), compared to control mice (mean 15.9%, median 15.4%, range 11.7–21.0%, $P = 0.0060$) (Fig. 4B, left panel). An example of calculating the percentage necrotic area is presented in Fig. 4B, right-hand panels. Bevacizumab treatment resulted in decreased vascular number in the tumor tissues [3.1, 2.6,

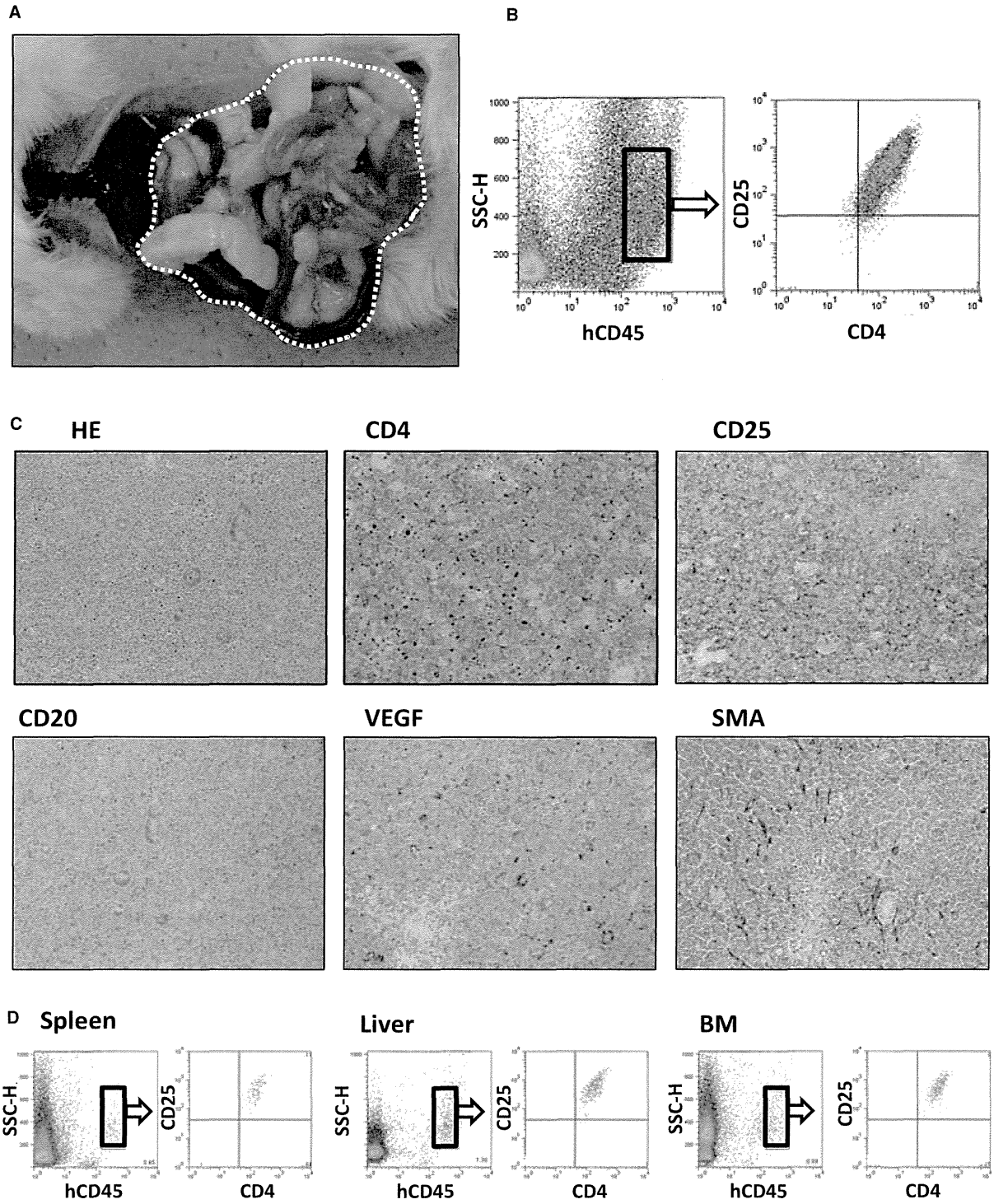

Figure 2 ATL cell-bearing NOG mouse model. (A) Macroscopic appearance of a primary DLBCL cell-bearing ATL mouse. The intraperitoneal mass is demarcated by a thin white dotted line. (B) Human CD45-positive cells in the mass determined by human CD4 and CD25 expression. (C) Immunohistochemical images of the intraperitoneal mass. (D) Human CD45-positive cells of each organ determined by human CD4 and CD25 expression.

0.0–8.3/mm^2; (mean, median, range)], compared to controls (12.8, 15.6, 1.6–19.3/mm^2, $P = 0.0127$) (Fig. 4C, left panel). An example of this calculation is presented in Fig. 4C, right-hand panels. Because sIL2R appears in the serum, concomitant with its increased expression on cells, we measured human sIL2R concentrations as a surrogate marker reflecting

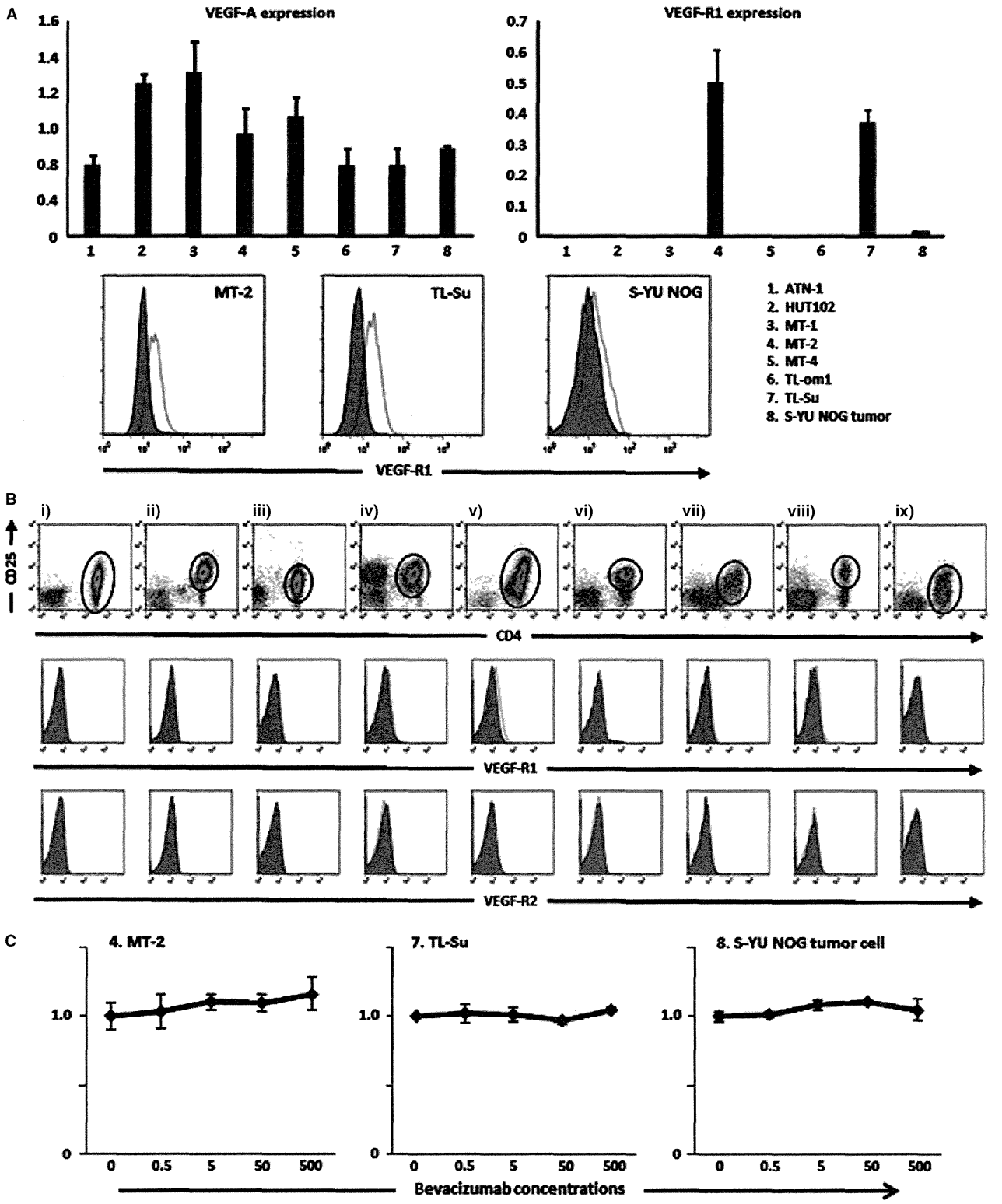

Figure 3 Vascular endothelial growth factor A (VEGF-A), VEGF-R1, and -R2 expression in primary ATL cells, or ATL and HTLV-1-immortalized lines (A) Quantitative RT-PCR analysis for VEGF-A and VEGF-R1 in 7 ATL and HTLV-1-immortalized lines, and NOG ATL cells from the intraperitoneal mass (upper panels). Flow cytometry for VEGF-R1 in HTLV-1-immortalized lines MT-2 and TL-Su, and NOG ATL cells, from the intraperitoneal mass (lower panels). (B) Flow cytometry for VEGF-R1, and -R2 in 9 primary ATL cells. (C) Bevacizumab has no direct anti-proliferative activity against HTLV-1-immortalized lines (MT-2 and TL-Su) expressing both VEGF-A and VEGF-R1, or NOG ATL cells, *in vitro*. Each result represents three independent experiments.

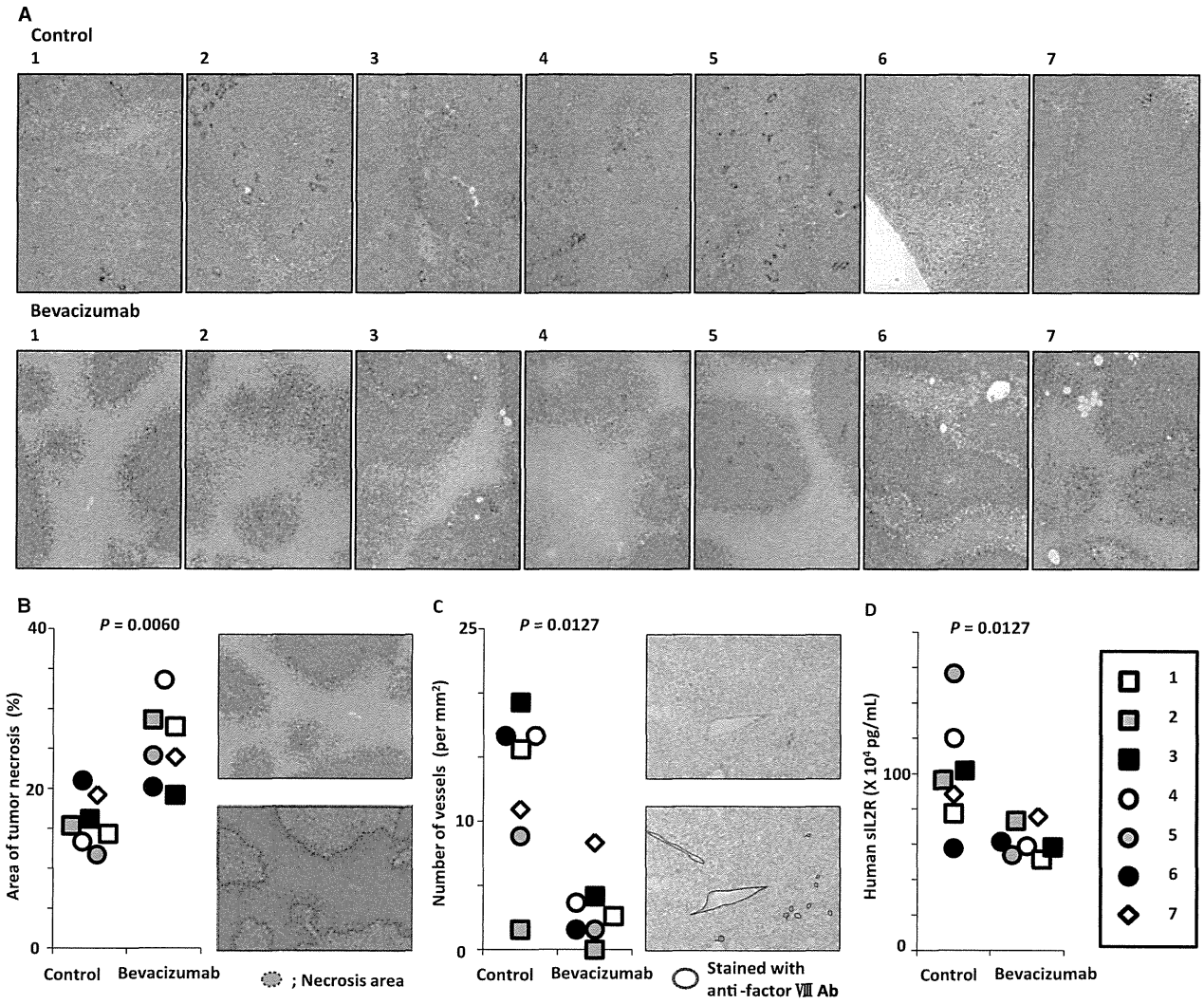

Figure 4 Bevacizumab therapy has significant therapeutic efficacy in the ATL cell-bearing NOG mouse model. (A) Macroscopic photomicrographs with hematoxylin and eosin staining of mice given saline (control) (upper panels) or bevacizumab (lower panels). (B) Area of tumor necrosis (%) of each ATL cell-bearing NOG mouse. The bevacizumab-treated mice had significantly greater tumor necrosis than control mice (left panel). An example of a calculation for tumor necrosis area (%) by means of Image J software is shown (right panels). (C) Numbers of vessels (/mm^2) of each ATL cell-bearing NOG mouse. The bevacizumab recipients had significantly fewer vessels than controls (left panel). An example of such a calculation by means of Image J software is shown (right panels). (D) Serum sIL2R concentrations of each ATL cell-bearing NOG mouse. The bevacizumab recipients had significantly lower levels of sIL2R than controls.

the tumor burden of the human CD25-expressing ATL (26). Treatment with bevacizumab showed significantly greater therapeutic efficacy as demonstrated by sIL2R concentrations in S-YU cell-bearing NOG mice (617.9, 588.5, 513.2–755.7 $\times$ 10^3 pg/mL), compared to controls (996.6, 963.4, 575.7–1565.0 $\times$ 10^3 pg/mL, P = 0.0127) (Fig. 4D). Although bevacizumab monotherapy showed significant therapeutic efficacy as demonstrated by the percentage of tumor necrosis, vascular number in the tumor tissues, and sIL2R concentrations in sera (Fig. 4), it did not confer any survival advantage to the NOG/S-YU mice (Fig. 5A). No toxicity attributable to bevacizumab injections was observed in any of the mice in this setting.

Therapeutic efficacy of bevacizumab plus CHOP compared to CHOP alone in S-YU cell-bearing NOG mice

The bevacizumab plus CHOP group did have a significant prolongation of survival compared with CHOP alone (P = 0.046). The median survival time of bevacizumab plus CHOP and CHOP alone was 38 and 34 d, respectively.

Discussion

In this study, we have demonstrated that bevacizumab possesses significant therapeutic efficacy in an ATL mouse model in which the tumor cells from a patient survive and

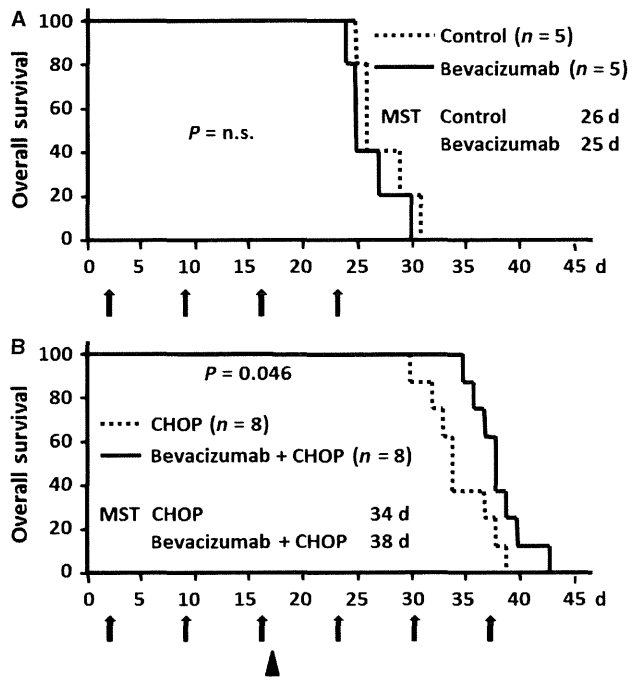

Figure 5 Survival analysis of ATL cell-bearing NOG mice treated with bevacizumab (A) Kaplan–Meier survival curves of ATL cell-bearing NOG mice treated with bevacizumab or saline. Arrows, bevacizumab or control (saline) injections. Each group consists of five mice. The difference between the bevacizumab and control groups is not significant. (B) Kaplan–Meier survival curves of ATL cell-bearing NOG mice treated with bevacizumab + CHOP, or CHOP alone. Arrows, bevacizumab or control (saline) injections. Arrow head, CHOP injection. Each group consists of eight mice. The difference between the bevacizumab + CHOP and CHOP alone is statistically significant.

proliferate in a murine microenvironment-dependent manner. The present finding revealed the importance of angiogenesis for the pathogenesis of VEGF-expressing ATL.

NOG mice have severe, multiple immune defects, such that human immune cells engrafted into them retain essentially the same functions as in humans (27, 28). While it has been reported that S-YU cells can be serially transplanted into SCID mice as recipients, the present study demonstrated that S-YU cells could also be serially transplanted into NOG mice. This was not unexpected given the even more severe immune dysfunction of NOG mice compared to SCID mice. This may also explain why the ATL tumor masses were much larger in NOG than in SCID mice.

In this study, most primary ATL cases (22/23), and all of the established cell lines tested (7/7), were positive for VEGF-A. These results are consistent with data from other investigators (16, 18, 19). Thus, the VEGF-A produced by ATL cells is likely to play an important role in the pathogenesis of ATL. On the other hand, *VEGF-R1 mRNA* expression was only seen in two of the seven ATL and HTLV-1-immortalized lines, and *VEGF–R2* in none of them. VEGF-R1 protein expression by primary ATL tumor cells was only seen in one of nine patients, and VEGF-R2 in none. In B-cell lymphomas, an earlier study reported that tumor cell growth was promoted in an autocrine fashion via VEGF-A/VEGF-R1 or VEGF-A/VEGF-R2 interactions (29). However, the present analysis of VEGF-R1/R2 expression in ATL, and the results of *in vitro* proliferation assays, did not support the existence of such an autocrine loop in ATL.

Because S-YU cells can only be maintained by serial transplantation in immunodeficient mice, but not by *in vitro* culture (30), the microenvironment is likely to be indispensable for their survival. S-YU are positive for VEGF-A, and therefore it would be expected that the interaction of VEGF-A produced by ATL cells with receptors on host (murine) endothelial cells should play an important role in tumor angiogenesis. This would lead to tumor cell survival and proliferation supported by transport of sufficient nutrients and oxygen in the mouse. Therefore, the present ATL model using S-YU should better reflect the human ATL *in vivo* environment, compared to other mouse models using established ATL cell lines, or HTLV-1-immortalized lines. Thus, this model should provide a powerful tool for understanding the pathogenesis of ATL. Furthermore, it should be useful not only for evaluating novel cytotoxic anti-ATL agents, but also provide a more appropriate *in vivo* model to test antitumor agents targeting the microenvironment, including bevacizumab.

The effect observed in mice receiving bevacizumab monotherapy, as demonstrated by the increased tumor necrosis area and reduced vasculature in the tumor tissue, was expected, given the conventional antitumor mechanism of bevacizumab, which neutralizes the human VEGF-A produced by the tumor cells, but not murine VEGF-A (31). It then inhibits the growth of new blood vessels and thus starves tumor cells of necessary nutrients and oxygen (32). This should lead to a reduced tumor burden, as indicated by the sIL2R concentrations measured. Although bevacizumab monotherapy did show this anti-angiogenesis effect, it did not lead to survival prolongation in this study. This finding is consistent with the clinical observations in many types of cancer such as colorectal cancer, non-small-cell lung cancer, renal cell carcinoma, and ovarian cancer. On the other hand, combination treatment with bevacizumab and CHOP did prolong survival compared to CHOP alone. Nonetheless, the extent of this prolongation was not marked, which is also consistent with clinical observations in many types of cancer where bevacizumab is of limited benefit and then only when combined with chemotherapy. This study suggested that the tumor cell 'starvation effect' alone mediated by bevacizumab does not result in prolonged survival. It has been reported that VEGF-targeted therapy can 'normalize' the tumor vascular network and that this can lead to a more uniform blood flow, with subsequent increased delivery of chemotherapeutic agents (33, 34). This normalization by bevacizumab is a possible explanation for the prolonged survival in the present combination setting.

The present study demonstrated the importance of angiogenesis for the pathogenesis of ATL and the potential efficacy of blocking this in at least a subgroup of patients with ATL. In recent clinical cancer therapy experience, the epidermal growth factor receptor (EGFR) tyrosine kinase inhibitor, gefitinib, failed to yield significantly improved overall survival in patients with refractory NSCLC, but did show therapeutic benefit in a subgroup of patients with mutated EGFR (35). In the case of mAb targeting the EGFR, both panitumumab and cetuximab also yield clinical benefits only in a subgroup of colorectal cancer patients with wild-type *KRAS* and BRAF (36). These findings indicate that we should develop novel treatment strategies based on tumor biology, and not on tumor category. Therefore, as a next step, further investigations are warranted to determine which subgroups of patients with ATL will benefit from bevacizumab therapy (37). In other words, we should face the challenge of developing robust biomarkers that can guide selection of those patients with ATL for whom bevacizumab therapy will be most beneficial. In addition, several promising new agents for treating ATL are currently being developed (1, 38–40). Investigations of combinations of bevacizumab with these novel agents are also warranted.

In conclusion, to the best of our knowledge this is the first report to evaluate the efficacy of bevacizumab for ATL in a tumor microenvironment-dependent animal model. Bevacizumab therapy combined with chemotherapy could be a potential treatment strategy for that subgroup of patients with ATL probably depending to a large extent on angiogenesis via VEGF for tumor survival and proliferation.

Acknowledgements

We thank Ms Chiori Fukuyama for her excellent technical assistance and Ms. Naomi Ochiai for her excellent secretarial assistance.

Funding

This study was supported by Grants-in-Aid for Scientific Research (B) (No. 25290058, T. Ishida), and Scientific Support Programs for Cancer Research (No. 221S0001, T. Ishida) from the Ministry of Education, Culture, Sports, Science and Technology of Japan, Grants-in-Aid for National Cancer Center Research and Development Fund (No. 21-6-3, T. Ishida), and H23-Third Term Comprehensive Control Research for Cancer-general-011, T. Ishida, from the Ministry of Health, Labour and Welfare, Japan.

Authorship contributions

Mori F, Ishida T, Asahi I, and Ueda R designed the research. Mori F, Ishida T, Asahi I, Sato F, Masaki A, Narita T, Suzuki S, Yamada T, and Takino H performed the research. Hishizawa M, Imada K, Takaori-Kondo A contributed to establishing the ATL mouse model. All the authors analyzed the data and wrote the article.

Conflict of interest

Nagoya City University Graduate School of Medical Sciences has received research funding for Takashi Ishida, Shigeru Kusumoto, and Shinsuke Iida from Chugai Pharmaceutical Co., Ltd. The other authors have no financial conflicts of interest related with this study.

References

1. Ishida T, Ueda R. Antibody therapy for adult T-cell leukemia-lymphoma. *Int J Hematol* 2011;**94**:443–52.
2. Matsuoka M, Jeang KT. Human T-cell leukaemia virus type 1 (HTLV-1) infectivity and cellular transformation. *Nat Rev Cancer* 2007;**7**:270–80.
3. Shimoyama M. Diagnostic criteria and classification of clinical subtypes of adult T-cell leukaemia-lymphoma. A report from the Lymphoma Study Group (1984–87). *Br J Haematol* 1991;**79**:428–37.
4. Uchiyama T, Yodoi J, Sagawa K, Takatsuki K, Uchino H. Adult T-cell leukemia: clinical and hematologic features of 16 cases. *Blood* 1977;**50**:481–92.
5. Ishida T, Hishizawa M, Kato K, *et al.* Allogeneic hematopoietic stem cell transplantation for adult T-cell leukemia-lymphoma with special emphasis on preconditioning regimen: a nationwide retrospective study. *Blood* 2012;**120**:1734–41.
6. Utsunomiya A, Miyazaki Y, Takatsuka Y, *et al.* Improved outcome of adult T cell leukemia/lymphoma with allogeneic hematopoietic stem cell transplantation. *Bone Marrow Transplant* 2001;**27**:15–20.
7. Carmeliet P, Jain RK. Molecular mechanisms and clinical applications of angiogenesis. *Nature* 2011;**473**:298–307.
8. Burger RA, Brady MF, Bookman MA, *et al.* Incorporation of bevacizumab in the primary treatment of ovarian cancer. *N Engl J Med* 2011;**365**:2473–83.
9. Escudier B, Pluzanska A, Koralewski P, *et al.* Bevacizumab plus interferon alfa-2a for treatment of metastatic renal cell carcinoma: a randomised, double-blind phase III trial. *Lancet* 2007;**370**:2103–11.
10. Escudier B, Bellmunt J, Négrier S, Bajetta E, Melichar B, Bracarda S, Ravaud A, Golding S, Jethwa S, Sneller V. Phase III trial of bevacizumab plus interferon alfa-2a in patients with metastatic renal cell carcinoma (AVOREN): final analysis of overall survival. *J Clin Oncol* 2010;**28**:2144–50.
11. Hurwitz H, Fehrenbacher L, Novotny W, *et al.* Bevacizumab plus irinotecan, fluorouracil, and leucovorin for metastatic colorectal cancer. *N Engl J Med* 2004;**350**:2335–42.
12. Perren TJ, Swart AM, Pfisterer J, *et al.* A phase 3 trial of bevacizumab in ovarian cancer. *N Engl J Med* 2011;**365**:2484–96.

13. Sandler A, Gray R, Perry MC, Brahmer J, Schiller JH, Dowlati A, Lilenbaum R, Johnson DH. Paclitaxel-carboplatin alone or with bevacizumab for non-small-cell lung cancer. *N Engl J Med* 2006;**355**:2542–50.
14. Yang JC, Haworth L, Sherry RM, Hwu P, Schwartzentruber DJ, Topalian SL, Steinberg SM, Chen HX, Rosenberg SA. A randomized trial of bevacizumab, an anti-vascular endothelial growth factor antibody, for metastatic renal cancer. *N Engl J Med* 2003;**349**:427–34.
15. Kreisl TN, Kim L, Moore K, *et al.* Phase II trial of single-agent bevacizumab followed by bevacizumab plus irinotecan at tumor progression in recurrent glioblastoma. *J Clin Oncol* 2009;**27**:740–5.
16. Bazarbachi A, Abou Merhi R, Gessain A, *et al.* Human T-cell lymphotropic virus type I-infected cells extravasate through the endothelial barrier by a local angiogenesis-like mechanism. *Cancer Res* 2004;**64**:2039–46.
17. El-Sabban ME, Merhi RA, Haidar HA, Arnulf B, Khoury H, Basbous J, Nijmeh J, de Thé H, Hermine O, Bazarbachi A. Human T-cell lymphotropic virus type 1-transformed cells induce angiogenesis and establish functional gap junctions with endothelial cells. *Blood* 2002;**99**:3383–9.
18. Hayashibara T, Yamada Y, Miyanishi T, Mori H, Joh T, Maeda T, Mori N, Maita T, Kamihira S, Tomonaga M. Vascular endothelial growth factor and cellular chemotaxis: a possible autocrine pathway in adult T-cell leukemia cell invasion. *Clin Cancer Res* 2001;**7**:2719–26.
19. Watters KM, Dean J, Gautier V, Hall WW, Sheehy N. Tax 1-independent induction of vascular endothelial growth factor in adult T-cell leukemia caused by human T-cell leukemia virus type 1. *J Virol* 2010;**84**:5222–8.
20. Ito M, Kobayashi K, Nakahata T. NOD/Shi-scid IL2rgnull (NOG) mice more appropriate for humanized mouse models. *Curr Top Microbiol Immunol* 2008;**324**:53–76.
21. Abramoff MD, Magelhaes PJ, Ram SJ. Image Processing with ImageJ. *Biophotonics Int* 2004;**11**:36–42.
22. Imada K, Takaori-Kondo A, Sawada H, Imura A, Kawamata S, Okuma M, Uchiyama T. Serial transplantation of adult T cell leukemia cells into severe combined immunodeficient mice. *Jpn J Cancer Res* 1996;**87**:887–92.
23. Suzuki S, Masaki A, Ishida T, *et al.* Tax is a potential molecular target for immunotherapy of adult T-cell leukemia/lymphoma. *Cancer Sci* 2012;**103**:1764–73.
24. Mori F, Ishida T, Ito A, *et al.* Potent antitumor effects of bevacizumab in a microenvironment-dependent human lymphoma mouse model. *Blood Cancer J* 2012;**2**:e67.
25. Mohammad RM, Wall NR, Dutcher JA, Al-Katib AM. The addition of bryostatin 1 to cyclophosphamide, doxorubicin, vincristine, and prednisone (CHOP) chemotherapy improves response in a CHOP-resistant human diffuse large cell lymphoma xenograft model. *Clin Cancer Res* 2000;**6**:4950–6.
26. Motoi T, Uchiyama T, Uchino H, Ueda R, Araki K. Serum soluble interleukin-2 receptor levels in patients with adult T-cell leukemia and human T-cell leukemia/lymphoma virus type-I seropositive healthy carriers. *Jpn J Cancer Res* 1988;**79**:593–9.
27. Ito A, Ishida T, Utsunomiya A, *et al.* Defucosylated anti-CCR4 monoclonal antibody exerts potent ADCC against primary ATLL cells mediated by autologous human immune cells in NOD/Shi-scid, IL-2R gamma(null) mice *in vivo*. *J Immunol* 2009;**183**:4782–91.
28. Masaki A, Ishida T, Suzuki S, *et al.* Autologous Tax-Specific CTL therapy in a primary adult T cell leukemia/lymphoma cell-bearing NOD/Shi-scid, IL-2Rγnull mouse model. *J Immunol* 2013;**191**:135–44.
29. Wang ES, Teruya-Feldstein J, Wu Y, Zhu Z, Hicklin DJ, Moore MA. Targeting autocrine and paracrine VEGF receptor pathways inhibits human lymphoma xenografts *in vivo*. *Blood* 2004;**104**:2893–902.
30. Koga H, Imada K, Ueda M, Hishizawa M, Uchiyama T. Identification of differentially expressed molecules in adult T-cell leukemia cells proliferating *in vivo*. *Cancer Sci* 2004;**95**:411–7.
31. Yu L, Wu X, Cheng Z, Lee CV, LeCouter J, Campa C, Fuh G, Lowman H, Ferrara N. Interaction between bevacizumab and murine VEGF-A: a reassessment. *Invest Ophthalmol Vis Sci* 2008;**49**:522–7.
32. Ellis LM, Hicklin DJ. VEGF-targeted therapy: mechanisms of anti-tumour activity. *Nat Rev Cancer* 2008;**8**:579–91.
33. Carmeliet P, Jain RK. Principles and mechanisms of vessel normalization for cancer and other angiogenic diseases. *Nat Rev Drug Discov* 2011;**10**:417–27.
34. Jain RK. Normalization of tumor vasculature: an emerging concept in antiangiogenic therapy. *Science* 2005;**307**:58–62.
35. Maemondo M, Inoue A, Kobayashi K, *et al.* Gefitinib or chemotherapy for non-small-cell lung cancer with mutated EGFR. *N Engl J Med* 2010;**362**:2380–8.
36. Bardelli A, Siena S. Molecular mechanisms of resistance to cetuximab and panitumumab in colorectal cancer. *J Clin Oncol* 2010;**28**:1254–61.
37. Lambrechts D, Lenz HJ, de Haas S, Carmeliet P, Scherer SJ. Markers of response for the antiangiogenic agent bevacizumab. *J Clin Oncol* 2013;**31**:1219–30.
38. Ishida T, Joh T, Uike N, *et al.* Defucosylated anti-CCR4 monoclonal antibody (KW-0761) for relapsed adult T-cell leukemia-lymphoma: a multicenter phase II study. *J Clin Oncol* 2012;**30**:837–42.
39. Tanosaki R, Tobinai K. Adult T-cell leukemia-lymphoma: current treatment strategies and novel immunological approaches. *Expert Rev Hematol* 2010;**3**:743–53.
40. Marçais A, Suarez F, Sibon D, Frenzel L, Hermine O, Bazarbachi A. Therapeutic options for adult T-cell leukemia/lymphoma. *Curr Oncol Rep* 2013;**15**:457–64.

Immunogenetics (2014) 66:161–170
DOI 10.1007/s00251-014-0760-y

ORIGINAL PAPER

Divergence and diversity of *ULBP2* genes in rhesus and cynomolgus macaques

Taeko K. Naruse · Hirofumi Akari · Tetsuro Matano · Akinori Kimura

Received: 10 November 2013 / Accepted: 13 January 2014 / Published online: 28 January 2014

Abstract Non-human primates such as rhesus macaque and cynomolgus macaque are important animals for medical research fields and they are classified as Old World monkey, in which genome structure is characterized by gene duplications. In the present study, we investigated polymorphisms in two genes for ULBP2 molecules that are ligands for NKG2D. A total of 15 and 11 *ULBP2.1* alleles and 11 and 10 *ULBP2.2* alleles were identified in rhesus macaques and cynomolgus macaques, respectively. Nucleotide sequences of exons for extra cellular domain were highly polymorphic and more than 70 % were non-synonymous variations in both *ULBP2.1* and *ULBP2.2*. In addition, phylogenetic analyses revealed that the *ULBP2.2* was diverged from a branch of *ULBP2.1* along with *ULBP2*s of higher primates. Moreover, when 3D structural models were constructed for the rhesus ULBP2 molecules, residues at presumed contact sites with NKG2D were polymorphic in *ULBP2.1* and *ULBP2.2* in the rhesus macaque and cynomolgus macaque, respectively. These observations suggest that amino acid replacements at the interaction sites with NKG2D might shape a specific nature of ULBP2 molecules in the Old World monkeys.

Keywords Rhesus macaque · Cynomolgus macaque · *ULBP2/RAET1H* · NKG2D · Polymorphisms

Introduction

Natural-killer group 2 member D (NKG2D), a C-type lectin molecule, is an activating receptor expressing on the surface of NK, $\gamma\delta^+$ and $CD8^+$ T cells, which plays an important role in the immune system (Wu et al., 1999; Raulet 2003). In humans, several MHC class I-like molecules are known as ligands for NKG2D, including MHC class I chain-related (MIC) and UL-16 binding protein (ULBP)/retinoic acid early transcript 1 (RAET1) (Bauer et al. 1999; Cosman et al. 2001; Chalupny et al. 2003; Bacon et al. 2004). These ligands are usually stress-inducible, and their recognition by NKG2D leads to the activation of NK cells, resulting in the killing of virus-infected cells and tumor cells (Pende et al. 2002; Eagle et al. 2006, Pappworth et al. 2007; Ward et al. 2007).

The human ULBP/RAET1 molecules are encoded by the *ULBP/RAET1* gene family located on the 6q24.2, which is composed of 10 members including six functional genes, *ULBP1*, *2*, *3*, *4*, *5*, and *6*, corresponding to *RAET1I*, *H*, *N*, *E*, *G*, and *L*, respectively (Radosavljevic et al. 2001; Chalupny et al. 2003; Eagle et al. 2009a, b; Eagle et al. 2009b). In addition, several sequence variations in each *ULBP* have been identified (Romphruk et al. 2009; Antoun et al. 2010). Although it is evident that the cell surface expression of the ligand molecules on target cells is differentially regulated (Eagle et al. 2006), genetic variations or polymorphisms in the coding region might also have a functional impact.

In the medical field, non-human primates including rhesus and cynomolgus macaques are used as animal models in the

Electronic supplementary material The online version of this article (doi:10.1007/s00251-014-0760-y) contains supplementary material, which is available to authorized users.

T. K. Naruse · A. Kimura (✉)
Department of Molecular Pathogenesis, Medical Research Institute, Tokyo Medical and Dental University (TMDU), 1-5-45 Yushima, Bunkyo-ku, Tokyo 113-8510, Japan
e-mail: akitis@mri.tmd.ac.jp

H. Akari
Primate Research Institute, Kyoto University, Inuyama, Japan

T. Matano
AIDS Research Center, National Institute of Infectious Diseases, Tokyo, Japan

T. Matano
The Institute of Medical Science, The University of Tokyo, Tokyo, Japan

immunological studies for infectious diseases, autoimmune diseases, organ transplantation, and development of vaccines. These macaques are members of the Old World monkey and it has been reported that the genetic diversity in the rhesus macaque is quite unique, i.e., more than 60 % of the rhesus macaque-specific expansions are found in the protein coding sequences (Gibbs et al. 2007). To fully evaluate the results of immunological experiments using macaque models, it is essential to characterize the genetic diversity of immune-related molecules, which may shape the basis of individual differences in the immune response against foreign antigens and/or pathogens. It has been reported that the copy numbers of genes in the major histocompatibility complex (MHC) loci in the Old World monkey are higher than those in humans (Kulski et al. 2004; Gibbs et al. 2007; Otting et al. 2007). In addition, the extent of genetic diversity in MHC differed, in part, depending on the geographic area, and we have reported that the diversity of MHC class I genes in the rhesus and cynomolgus macaques is considerably different depending on habitat (Naruse et al. 2010, Saito et al. 2012). In our previous study, we have demonstrated that *ULBP4* is more polymorphic in the Old World monkey than in humans (Naruse et al. 2011). It also was revealed that each member of the *ULBP/RAET1* gene family, except for *ULBP6*, had been duplicated in the rhesus genome (Naruse et al. 2011).

Recent reports have indicated that the expression of *ULBP2* is upregulated in HIV infection (Richard et al. 2013, Matusali et al. 2013). Because the innate immune system may be involved in the response to environmental pathogens, it is important to investigate the polymorphisms in the ligands of NK receptors in the experimental animal models for developing HIV vaccine. Here, we report the *ULBP2* polymorphisms focusing on the divergence and diversity in the Old World monkey.

Materials and methods

Animals

A total of 37 rhesus macaques and 24 cynomolgus macaques, previously analyzed for the polymorphisms in MHC class I genes (Naruse et al. 2010, Saito et al. 2012) were the subjects. They were maintained in the breeding colonies in Japan. The founders of the rhesus macaque colonies were captured in Myanmar and Laos, whereas the founders of cynomolgus macaque colonies were captured in Indonesia, Malaysia, and the Philippines. All care including blood sampling of animals were in accordance with the guidelines for the Care and Use of Laboratory Animals published by the National Institutes of Health (NIH publication 85-23, revised 1985) and the study protocol was subjected to prior approval by the local animal protection authority.

DNA extraction and sequencing analysis

Genomic DNAs of B lymphoblastoid cell lines from rhesus macaques and whole blood samples of cynomolgus macaques were prepared, as previously reported (Naruse et al. 2010, Saito et al. 2012). Amplification of *ULBP2* from macaques was done by polymerase chain reaction (PCR) with specific primer pairs designed for the region spanning from intron 1 to intron 3 of rhesus *ULBP2*, LOC694466 (designated as *ULBP2.1*) and LOC694600 (designated as *ULBP2.2*), using FastStart Taq DNA polymerase (Roche, Mannheim, Germany). Primer sequences are as follows: UL2.1NF (5′-AGGGGCTAACTAGGGGTCTTTC) and UL2.1NR (5′ ACCGTTTCTGATCTCATTCCA) for *ULBP2.1*, and UL2.2NF (5′-GAGGGCTAACTAGGGGTCTCT) and UL2.2NR (5′-ACCATTTCTGATCTCATTCCAGA) for *ULBP2.2*. The PCR program was composed of following steps: denaturation at 95 °C for 4 min; 30 cycles of 95 °C for 30 s, 56 °C for 30 s, 72 °C for 45 s; and additional extension at 72 °C for 7 min. The PCR products, about 1,400 bp for *ULBP2.1* and about 1,080 bp for *ULBP2.2*, were cloned into pSTBlue-1 AccepTer vector (Novagen, WI, USA) according to the manufacturer's instructions and transformed into Nova Blue Single™ competent cells (Merck Biosciences Japan, Tokyo, Japan). Ten to 20 independent transformed colonies were picked up for each sample and subjected to sequencing on both strands by using a BigDye Terminator cycling system and an ABI 3730 automated sequence analyzer (Applied Biosystems, CA, USA).

Data analysis

Nucleotide sequences from cloned DNAs were aligned using the Genetyx software package (version 8.0, Genetyx Corp., Japan). When at least three clones from independent PCR or from different subjects showed identical sequences, the sequences were submitted to the DNA Data Bank of Japan (DDBJ). A neighbor-joining tree was constructed by Kimura's two-parameter method for a phylogenetic analysis of *ULBP2* sequences from exon 2 to exon 3, excluding intron 2 sequences, by using the Genetyx software. Bootstrap values were based on 5,000 replications. The *ULBP2* and *ULBP6* sequences from human (GenBank accession numbers AL583835 and AL355497, respectively), and *ULBP2* sequences from chimpanzee (NC006473), western gorilla (NC018430), rhesus (NC007861), and another member of Old World monkey, olive baboon (NC018155) were included in the phylogenetic analysis. The *ULBP1* (LOC694341), *ULBP3* (LOC694525), *ULBP4* (LOC695031), and *ULBP5* (LOC694265) sequences from rhesus macaque, and *ULBP1* (NM025218), *ULBP3* (AL355497), *ULBP4* (AL355312), and *ULBP5* (AL583835) sequences from human were also included in the analysis.

Table 1 Alleles of *ULBP2.1* and *ULBP2.2* in rhesus and cynomolgus macaques

Gene	Species	Allele name	Accession no	ID of reference animal	Clone name
ULBP2.1	*Macaca mulatta*	*Mamu-ULBP2.1*1*	NC007861[a]	Not found in the subjects of this study	
		*Mamu-ULBP2.1*2*	AB826205	R491	UL2.1NR491F-9
		*Mamu-ULBP2.1*3*	AB826206	R312, R314, R496	UL2.1NR314F-2
		*Mamu-ULBP2.1*4*	AB826207	R277, R316, R350, R396, R429, R434, R437, R455, R465, R473, R492, R495	UL2-1R227-13 F
		*Mamu-ULBP2.1*5*	AB826208	R325, R333, R337, R384, R434, R491	UL2-1R434-2 F
		*Mamu-ULBP2.1*6*	AB826209	R350	UL2.1NR350F-13
		*Mamu-ULBP2.1*7*	AB826210	R227, R234, R283, R314, R320, R321, R328, R337, R346, R384,R396, R446, R455, R465, R490, R496	UL2-1R227-7 F
		*Mamu-ULBP2.1*8*	AB826211	R495	UL2.1NR495F-8
		*Mamu-ULBP2.1*9*	AB826212	R321, R333, R360	UL2.1NR321F-8
		*Mamu-ULBP2.1*10*	AB826213	R316, R342, R408	UL2-1R408-12 F
		*Mamu-ULBP2.1*11*	AB826214	R346	UL2.1NR346F-20
		*Mamu-ULBP2.1*12*	AB826215	R342	UL2.1NR342F-14
		*Mamu-ULBP2.1*13*	AB826216	R325, R346, R360, R361, R379, R408, R429, R430, R437, R439, R446, R473, R490	UL2.1NR439F-11
		*Mamu-ULBP2.1*14*	AB826217	R453	UL2-1R453-1 F
		*Mamu-ULBP2.1*15*	AB826204	R234, R312, R361	UL2.1NR234F-7
	Macaca fascicularis	*Mafa-ULBP2.1*1*	NC007861[a]	M04, C09	2.1-2UL2-1 M04-5 F
		*Mafa-ULBP2.1*2*	AB826219	M05, C10, C11	UL2.1NFM05-12
		*Mafa-ULBP2.1*3*	AB826220	M03, C07	UL2.1NFM03-8
		*Mafa-ULBP2.1*4*	AB826221	P01, P02, P03, M01, C01, C03, C04, C05, C07, C08	2.1-1UL2-1 M01-10 F
		*Mafa-ULBP2.1*5*	AB826222	P02, C06	UL2-1P02-2 F
		*Mafa-ULBP2.1*6*	AB826223	M02, C05	2.1-6UL2-1 M02-17 F
		*Mafa-ULBP2.1*7*	AB826224	M03, M04, C06, C08, C09	UL2-1 M03-1 F
		*Mafa-ULBP2.1*8*	AB826225	P04, P05, M01, M05, M06, C02, C12, C13	2.1-3UL2-1 M01-12 F
		*Mafa-ULBP2.1*9*	AB826226	P04, M06, C10, C11, C12, C13	2.1-4UL2-1 M06-10 F
		*Mafa-ULBP2.1*10*	AB826228	M02, C04	UL2-1 M02-20 F
		*Mafa-ULBP2.1*11*	AB826218	P01, C02	UL2NP01-F-2
ULBP2.2	*Macaca mulatta*	*Mamu-ULBP2.2*1*	NC007861[b]	R283, R316, R320, R321, R325, R328, R333, R337, R342, R346, R360, R379, R384, R396, R408, R429, R430, R437, R439, R446, R453, R473, R490, R495	UL2-2R396-3 F
		*Mamu-ULBP2.2*2*	AB827340	R491	UL2.2NR491F-5
		*Mamu-ULBP2.2*3*	AB827341	R314, R321	UL2-2R314-7 F
		*Mamu-ULBP2.2*4*	AB827342	R350	UL2.2NR350F-3
		*Mamu-ULBP2.2*5*	AB827343	R234, R320	UL2-2R361-8 F
		*Mamu-ULBP2.2*6*	AB827344	R325, R333, R337, R384, R491, R492	UL2-2R325-12 F
		*Mamu-ULBP2.2*7*	AB827345	R237, R312, R453	UL2-2R237-5 F
		*Mamu-ULBP2.2*8*	AB827346	R228, R314, R396, R492, R495	UL2-2R383-3 F
		*Mamu-ULBP2.2*9*	AB827347	R496	UL2-2R496-12 F
		*Mamu-ULBP2.2*10*	AB827339	R234, R312, R328, R439,R446, R490, R496	R234UL2.2NF-16
		*Mamu-ULBP2.2*11*	AB827348	R367, R430	UL2-2R367-12 F

Table 1 (continued)

Gene	Species	Allele name	Accession no	ID of reference animal	Clone name
	Macaca fascicularis	*Mafa-ULBP2.2*1*	NC007861[b]	M05, C10, C11	UL2-2FM05-2
		*Mafa-ULBP2.2*2*	AB827350	M03, M04, C06, C08	UL2-2FM03-1
		*Mafa-ULBP2.2*3*	AB827351	P03, C08	P03UL2-2-6 F
		*Mafa-ULBP2.2*4*	AB827352	P01, C03, C04, C05	UL2-2P01-1 F
		*Mafa-ULBP2.2*5*	AB827353	P01,P03, P04, M01, M04, M06, C01, C02, C09, C11, C13	UL2-2P01-7 F
		*Mafa-ULBP2.2*6*	AB827354	P04, P05, M05, M06, C12, C13	UL2-2P04-19 F
		*Mafa-ULBP2.2*7*	AB827355	M02, C05,	UL2-2FM02-2
		*Mafa-ULBP2.2*8*	AB827356	M03, C07	UL2-2FM03-11
		*Mafa-ULBP2.2*9*	AB828102	P02, M01, C01, C03, C06, C07	UL2-2FM01-1
		*Mafa-ULBP2.2*10*	AB827349	M02, C04	UL2-2FM02-11

[a] Identical to LOC694466

[b] Identical to LOC694600

Structure model analysis

Three-dimensional (3D) structure models of ULBP2 molecules were created for amino acid positions from 1 to191, by using a molecular visualization software RasTop2.2 (http://sourceforge.net/projects/rastop/), by referring the human ULPB3 molecule in complex with NKG2D (Radaev et al. 2001) from the Molecular Modeling Database (MMCB No.18231). Polymorphic sites were mapped on the 3D structure models by using the Cn3D 4.1 program (http://www.ncbi.nlm.nih.gov/Structure/CN3D/cn3d.shtml).

Results

Identification of alleles for a ULBP2 gene, *ULBP2.1*

There are two orthologous genes for *ULBP2*, LOC694466 and LOC694600, in the rhesus macaque genome. In the present study, we designated LOC694466 and LOC694600 as *ULBP2.1* and *ULBP 2.2*, respectively, and we designed primer pairs to separately amplify the *ULBP2.1* and *ULBP 2.2*. As expected, PCR products from each gene could be obtained and distinguished by their lengths, although minor length differences due to single nucleotide repeat number polymorphisms in an A stretch were found in the intron 2 sequences.

We obtained nucleotide sequences for the region from exon 2 to exon 3 of *ULBP2.1* from 37 rhesus macaques and 24 cynomolgus macaques by sequencing the cloned PCR products of 1,370–1,395 bp. The *ULBP2.1* sequences from the rhesus macaques were classified into 15 different alleles (Table 1), designated as *Mamu-ULBP2.1*1* to *-ULBP2.1*15*. The LOC4964466 sequences were given with the allele name of *Mamu-ULBP2.1*1*, although it was not found in the analyzed subjects of current study. In the cynomolgus macaques, 11 different alleles, *Mafa-ULBP2.1*01* to *-ULBP2.1*11*, were identified (Table 1). The nucleotide sequences of *Mafa-ULBP2.1*1* were identical to those of *Mamu-ULBP2.1*1* reported for rhesus macaque LOC694466.

Fig. 1 Phylogenetic tree of *ULBP2.1* and *ULBP2.2* alleles and related *ULBP2*. The tree was constructed using neighbor-joining method with bootstrap values of 5,000 replications. The values are indicated as percentages and those values less than 50 % are not shown. The sequences of human *ULBP2* (AY026825), human *ULBP5* (AL583835), human *ULBP6* (AL355497), rhesus *ULBP5* (LOC694265), chimpanzee *ULBP2* (NC006473), western gorilla *ULBP2* (NC018430), and olive baboon *ULBP2* (NC018155) were included in the analysis. The *underlined alleles* indicated with *triangles* and *stars* carried polymorphisms on the α helix structure and contact sites with NKG2D, respectively ▶

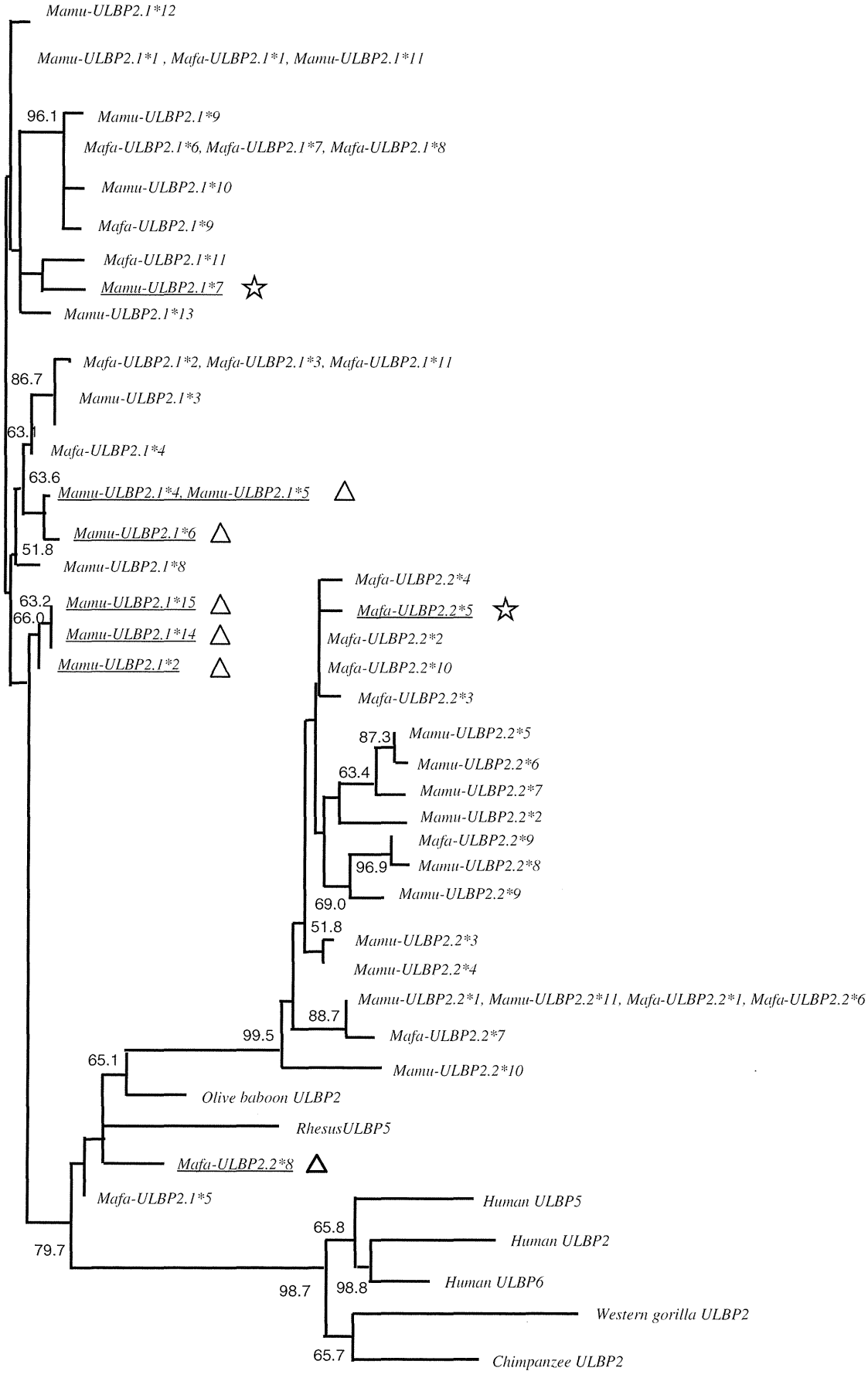
Mamu-ULBP2.1*12
Mamu-ULBP2.1*1 , Mafa-ULBP2.1*1, Mamu-ULBP2.1*11
96.1
Mamu-ULBP2.1*9
Mafa-ULBP2.1*6, Mafa-ULBP2.1*7, Mafa-ULBP2.1*8
Mamu-ULBP2.1*10
Mafa-ULBP2.1*9
Mafa-ULBP2.1*11
Mamu-ULBP2.1*7
Mamu-ULBP2.1*13
Mafa-ULBP2.1*2, Mafa-ULBP2.1*3, Mafa-ULBP2.1*11
86.7
Mamu-ULBP2.1*3
63.1
Mafa-ULBP2.1*4
63.6
Mamu-ULBP2.1*4, Mamu-ULBP2.1*5
Mamu-ULBP2.1*6
51.8
Mamu-ULBP2.1*8
63.2
Mamu-ULBP2.1*15
66.0
Mamu-ULBP2.1*14
Mamu-ULBP2.1*2
Mafa-ULBP2.2*4
Mafa-ULBP2.2*5
Mafa-ULBP2.2*2
Mafa-ULBP2.2*10
Mafa-ULBP2.2*3
87.3
Mamu-ULBP2.2*5
Mamu-ULBP2.2*6
63.4
Mamu-ULBP2.2*7
Mamu-ULBP2.2*2
Mafa-ULBP2.2*9
96.9
Mamu-ULBP2.2*8
Mamu-ULBP2.2*9
69.0
51.8
Mamu-ULBP2.2*3
Mamu-ULBP2.2*4
Mamu-ULBP2.2*1, Mamu-ULBP2.2*11, Mafa-ULBP2.2*1, Mafa-ULBP2.2*6
88.7
Mafa-ULBP2.2*7
99.5
Mamu-ULBP2.2*10
65.1
Olive baboon ULBP2
RhesusULBP5
Mafa-ULBP2.2*8
Mafa-ULBP2.1*5
Human ULBP5
65.8
Human ULBP2
79.7
98.8
Human ULBP6
98.7
Western gorilla ULBP2
65.7
Chimpanzee ULBP2

Table 2 Number of polymorphic sites and non-synonymous sites in ULBP2 genes in macaques and human

Locus	Number of alleles	Exon 2		Intron 2	Exon 3	
		Polymorphic sites	Non-synonymous sites (%)	Polymorphic sites	Polymorphic sites	Non-synonymous sites (%)
Mamu ULBP2.1	15	10	10 (100)	14	7	4 (57.1)
Mafa ULBP2.1	11	8	7 (87.5)	12	6	3 (50.0)
Mamu ULBP2.2	11	7	6 (85.7)	9	14	9 (64.3)
Mafa ULBP2.2	10	17	7 (41.2)	13	12	9 (75.0)
Human ULBP2	NC	17	14 (82.3)	0	15	11 (74.0)
Human ULBP6	NC	14	13 (92.9)	1	17	11 (64.7)

NC not counted because the polymorphisms in the public databases are indicated for each site and not for full sequence

Identification of alleles for another ULBP2 gene, *ULBP2.2*

PCR products for *ULBP2.2* could be obtained from genomic DNAs of both rhesus and cynomolgus macaques. Sequencing data from the cloned PCR products of 1,080–1,085 bp were classified into 11 different alleles, *Mamu-ULBP2.2*1* to *-ULBP2.2*11*, from the rhesus macaques and 10 alleles, *Mafa-ULBP2.2*1* to *-ULBP2.2*10*, from the cynomolgus

a

```
Mamu-ULBP2.1*1     1:PRWSQTGGDD PHSLCYDITI IPKFRPGPQW CAVQGQVDKK TFLHYDCGNK TVTSVSPLGK KLNVTKAWKA QNPVLREVVD MLTEQLLDIQ LENYTPREPL 100
Mamu-ULBP2.1*2      :********** ---------- ---------- ---------- ---------- ---------- ---------- ---------- ---------- ----------
Mamu-ULBP2.1*3      :********** ---------- ---------- ---------- ---------- ---------- ---------- ---------- ---------E ----------
Mamu-ULBP2.1*4      :********** ---------- ---------- ---------- ---------- ---------- ---------- ---------- ---------- ----------
Mamu-ULBP2.1*5      :********** ---------- ---------- ---------- ---------- ---------- ---------- ---------- ---------- ----------
Mamu-ULBP2.1*6      :********** L--------- ---------- ---------- ---------- ---------- ---------- ---------- ---------- ----------
Mamu-ULBP2.1*7      :********** ---------- --------R- ---------- ---------- ---------- ---------- --T------- ---------- ----------
Mamu-ULBP2.1*8      :********** ---------- ---------- ---------- ---------- ------T--- ---------- ---------- ---------- ----------
Mamu-ULBP2.1*9      :********** L--------- ---------- ---------- ---------- ----I-T--- ---------- ---------- ---------- ----------
Mamu-ULBP2.1*10     :********** L--------- ---------- Y--------- ---------- ------T--- ---------- ---------- ---------- ----------
Mamu-ULBP2.1*11     :********** ---------- ---------- ---------- ---------- ---------- ---------- ---------- ---------- ----------
Mamu-ULBP2.1*12     :********** ---------- ---------- ---------- ---------- ---------- ---------- ---------- ---------- ----------
Mamu-ULBP2.1*13     :********** ---------- ---------- ---------- ---------- ---P------ ---------- ---------- ---------- ----------
Mamu-ULBP2.1*14     :********** ---------- ---------- ---------- ---------- ---------- Q--------- ---------- ---------- ----------
Mamu-ULBP2.1*15     :********** ---------- ---------- ---------- ---------- ---------- Q--------- ---------- ---------- ----------
Mafa-ULBP2.1*1      :********** ---------- ---------- ---------- ---------- ---------- ---------- ---------- ---------- ----------
Mafa-ULBP2.1*2      :********** ---------- ---------- ----D----- ---------- ---------- ---------- ---------- ---------E ----------
Mafa-ULBP2.1*3      :********** ---------- ---------- ----D----- ---------- ---------- ---------- ---------- ---------E ----------
Mafa-ULBP2.1*4      :********** ---------- ---------- ---------- ---------- ---------- ---------- ---------- ---------- ----------
Mafa-ULBP2.1*5      :********** L--------- --------R- ---------- ---------- ---P------ ---------- ---------- ---------- ----------
Mafa-ULBP2.1*6      :********** L--------- ---------- ---------- ---------- ------T--- ---------- ---------- ---------- ----------
Mafa-ULBP2.1*7      :********** L--------- ---------- ---------- ---------- ------T--- ---------- ---------- ---------- ----------
Mafa-ULBP2.1*8      :********** L--------- ---------- ---------- ---------- ------T--- ---------- ---------- ---------- ----------
Mafa-ULBP2.1*9      :********** L-------I- ---------- ---------- ---------- ------T--- ---------- ---------- ---------- ----------
Mafa-ULBP2.1*10     :********** ---------- --------R- ----D----- ---------- ------T--- ---------- ---------- ---------- ----------
Mafa-ULBP2.1*11     :********** ---------- ---------- ---------- ---------- ---------- ---------- ---------- ---------E ----------
Mamu-ULBP2.2*1      :SL--RA-RA- L-----E--- -------RR- ---------- ---------- I--P------ --S------- ---------- ---------- ----------
Mamu-ULBP2.2*2      :********** L-----E--- -------RR- ---------- ---------- I--P----V- -FS------- ---------- ---------- ----------
Mamu-ULBP2.2*3      :********** L-----E--- -------RR- ---------- ---------- I--P------ -FS------- ---------- ---------- ----------
Mamu-ULBP2.2*4      :********** L-----E--- -------RR- ---------- ---------- I--------- -FS------- ---------- ---------- ----------
Mamu-ULBP2.2*5      :********** L-----E--- -------RR- ---------- ---------- I--PI----- -FS------- ---------- ---------- ----------
Mamu-ULBP2.2*6      :********** L-----E--- -------RR- ---------- ---------- I--PI---V- -FS------- ---------- ---------- ----------
Mamu-ULBP2.2*7      :********** L-----E--- -------RR- ---------- ---------- I--PI----- -FS------- ---------- ---------- ----------
Mamu-ULBP2.2*8      :********** L-----E--- -------RR- ---------- ---------- I--P------ -FS------- ---------- ---------- ----------
Mamu-ULBP2.2*9      :********** L-----E--- -------RR- ---------- ---------- ---P------ -FS------- ---------- ---------- ----------
Mamu-ULBP2.2*10     :********** L-----E--- -------RR- ---------- ------Y--- I--P------ -LS------- ---------- ---------- ----------
Mamu-ULBP2.2*11     :********** L-----E--- -------RR- ---------- ---------- I--P------ -LS------- ---------- ---------- ----------
Mafa-ULBP2.2*1      :********** L-----E--- -------RR- ---------- ---------- I--P------ -LS------- ---------- ---------- ----------
Mafa-ULBP2.2*2      :********** L-----E--- -------RR- ---------- ---------- I--P------ -FS------- ---------- ---------- ----------
Mafa-ULBP2.2*3      :********** L-----E--- -------RR- ---------- ---------- I--P------ -FS------- ---------- ---------- ----------
Mafa-ULBP2.2*4      :********** L-----E--- -------RR- ---------- ---------- I--P------ -FS------- ---------- ---------- ----------
Mafa-ULBP2.2*5      :********** L-----E--- -------RR- ---------- ---------- I--P------ -FS------- ---------- ---------- ----------
Mafa-ULBP2.2*6      :********** L-----E--- -------RR- ---------- ---------- I--P------ --S------- ---------- ---------- ----------
Mafa-ULBP2.2*7      :********** L-----E--- -------RR- ---------- ---------- I--P------ --S------- ---------- ---------- ----------
Mafa-ULBP2.2*8      :********** ---------- -------PR- ---------- ---------- ---P--T--- ---------- ---------- ---------- ----------
Mafa-ULBP2.2*9      :********** L-----E--- -------RR- ---------- ---------- I--P------ -FS------- ---------- ---------- ----------
Mafa-ULBP2.2*10     :********** L-----E--- -------RR- ---------- ---------- I--P------ -FS------- ---------- ---------- ----------
Human ULBP2         :SG--RA-RA- ------D--V -------PR- --------E- ---------- ---P------ -----T---- ---------- I-----R--- ------K---
Human ULBP6         :FG--RARR-- ------D--V -------PR- --------E- ---------- ---P------ -----M---- ---------- I--------- ------K---
```

Fig. 2 Alignment of deduced amino acid sequences of α1 and α2 domains of ULBP2-related molecules from rhesus and cynomolgus macaques and human. Amino acid sequences deduced from nucleotide sequences for *Mamu-ULBP2.1*1* and alleles of *Mamu-ULBP2.1*, *Mafa-ULBP2.1*, *Mamu-ULBP2.2,* and *Mafa-ULBP2.2*, were aligned with human *ULBP2* (AY026825), and *ULBP6* (AL355497). *Numbers* represent the amino acid positions in mature protein. Sequences for the predicted α helix structure are *underlined* and *contact sites* with NKG2D are *boxed* in the *Mamu-ULBP2.1*1* sequences. *Dashes* indicate identity to the *Mamu-ULBP2.1*1* sequences. *Asterisks* represent not sequenced regions. Amino acid sequences are shown **a** from 1 to 100 and **b** from 101 to 191

b

```
Mamu-ULBP2.1*1   101:TLQARMSCEQ KAEGHSSGSW QFGFDGQVFL LFDSENRMWT TVHPGARKMK EKWENDKDVT MSFHYISMGD CTRWLGDFLM DMDSTLEPSA G 191
Mamu-ULBP2.1*2       :---------- ---------- ---------- ---------- ---------- ---------- ---------- ---------- G--------- -
Mamu-ULBP2.1*3       :---------- ---------- ---------- ---------- ---------- ---------- ---------- ---------- ---------- -
Mamu-ULBP2.1*4       :---------- ---------- ---------- ---------- ---------- ---------- ---------- ------E--- ---------- -
Mamu-ULBP2.1*5       :---------- ---------- ---------- ---------- ---------- ---------- ---------- ------E--- ---------- -
Mamu-ULBP2.1*6       :---------- ---------- ---------- ---------- ---------- ---------- ---------- ------E--- ---------- -
Mamu-ULBP2.1*7       :---------- ---------- ---------- ---------- ---------- ---------- ---------- ---------- ---------- -
Mamu-ULBP2.1*8       :---------- ---------- ---------- ---------- ---------- ---------- ---------- ---------- ---------- -
Mamu-ULBP2.1*9       :----------T---------- ---------- ---------- ---------- ---------- ---------- ---------- ---------- -
Mamu-ULBP2.1*10      :----------T---------- ---------- ---------- ---------- ---------- ---------- ---------- ---------- -
Mamu-ULBP2.1*11      :---------- ---------- ---------- ---------- ---------- ---------- ---------- ---------- ---------- -
Mamu-ULBP2.1*12      :---------- ---------- ---------- ---------- --------I- ---------- ---------- ---------- ---------- -
Mamu-ULBP2.1*13      :---------- ---------- ---------- ---------- ---------- ---------- ---------- ---------- ---------- -
Mamu-ULBP2.1*14      :---------- ---------- ---------- ---------- ---------- ---------- ---------- ---------- G--------- -
Mamu-ULBP2.1*15      :---------- ---------- ---------- ---------- ---------- ---------- ---------- ---------- G--------- -
Mafa-ULBP2.1*1       :---------- ---------- ---------- ---------- ---------- ---------- ---------- ---------- ---------- -
Mafa-ULBP2.1*2       :---------- ---------- ---------- ---------- ---------- ---------- ---------- ---------- ---------- -
Mafa-ULBP2.1*3       :---------- ---------- ---------- ---------- ---------- ---------- ---------- ---------- ---------- -
Mafa-ULBP2.1*4       :---------- ---------- ---------- ---------- ---------- ---------- ---------- ---------- ---------- -
Mafa-ULBP2.1*5       :-----V---- ---------- ---------- ---------- ---------- ---------- ---------- ---------- ---------- -
Mafa-ULBP2.1*6       :----------T---------- ---------- ---------- ---------- ---------- ---------- ---------- ---------- -
Mafa-ULBP2.1*7       :----------T---------- ---------- ---------- ---------- ---------- ---------- ---------- ---------- -
Mafa-ULBP2.1*8       :----------T---------- ---------- ---------- ---------- ---------- ---------- ---------- ---------- -
Mafa-ULBP2.1*9       :----------T---------- ---------- ---------- ---------- ---------- ---------- ---------- ---------- -
Mafa-ULBP2.1*10      :----------- -----R---- ---------- ---------- ---------- ---------- ---------- ---------- ---------- -
Mafa-ULBP2.1*11      :---------- ---------- ---------- ---------- ---------- ---------- ---------- ---------- ---------- -
Mamu-ULBP2.2*1       :-----V---- -----R---- ---------- ---------- ---------- ---------- ---------- -----K---T GT-------- -
Mamu-ULBP2.2*2       :----QV---- ---------- ---------- ---------- M--------- ---Q------ ---------- -----K---- G--------- -
Mamu-ULBP2.2*3       :-----V---- ---------- ---------- ---------- ---------- ---------- ---R------ -----K---- G--------- -
Mamu-ULBP2.2*4       :-----V---- ---------- ---------- ---------- ---------- ---------- ---R------ -----K---- G--------- -
Mamu-ULBP2.2*5       :-----V---- ----------  --S------- ---------- ---------- ---------- ---------- -----K---T GT-------- -
Mamu-ULBP2.2*6       :-----V---- ----------  --S------- ---------- ---------- ---------- ---------- -----K---T GT-------- -
Mamu-ULBP2.2*7       :-----V---- -----R---- ---------- ---------- ---------- ---------- ---------- -----K---T GT-------- -
Mamu-ULBP2.2*8       :----QV---- ---------- ---------- ---------- ---------- ------R--- ---------- -----K---T GM-------- -
Mamu-ULBP2.2*9       :----QV---- ---------- ---------- ---------- ---------- ------R--- ---------- -----K---T GT-------- -
Mamu-ULBP2.2*10      :----QV---- ---------- ---------- ---------- M--------- ---Q------ ---------- -----K---T G--------- -
Mamu-ULBP2.2*11      :-----V---- -----R---- ---------- ---------- ---------- ---------- ---------- -----K---T GT-------- -
Mafa-ULBP2.2*1       :-----V---- -----R---- ---------- ---------- ---------- ---------- ---------- -----K---T GT-------- -
Mafa-ULBP2.2*2       :-----V---- ---------- ---------- ---------- ---------- ---------- ---------- -----K---- G--------- -
Mafa-ULBP2.2*3       :-----V---- ---------- ---------- ---------- ---------- ---------- ---------- -----K---- G--------- -
Mafa-ULBP2.2*4       :-----V---- ---------- ---------- ---------- ---------- ---------- ---------- -----K---- G--------- -
Mafa-ULBP2.2*5       :-----V---- ---------- ---------- ---------- ---------- ---------- ---------- -----K---- G--------- -
Mafa-ULBP2.2*6       :-----V---- -----R---- ---------- ---------- ---------- ---------- ---------- -----K---T GT-------- -
Mafa-ULBP2.2*7       :-----V---- -----R---- ---------- ---------- ---------- ---Q------ ---------- -P---K---T GT-------- -
Mafa-ULBP2.2*8       :-----V---- ---------- ---------- ---------- ---------- -------N-- ---------- -----K---T ---------- -
Mafa-ULBP2.2*9       :----QV---- ---------- ---------- ---------- ---------- ------R--- ---------- -----K---T G--------- -
Mafa-ULBP2.2*10      :-----V---- ---------- ---------- ---------- ---------- ---------- ---------- -----K---- G--------- -
Human ULBP2          :---------- ---------- --S----I-- -----K---- ---------- -------V-A -----F---- -IG--E---- G--------- -
Human ULBP6          :---------- ---------- --SI---T-- -----K---- ---------- ---------A ---------- -IG--E---- G--------- -
```

Fig. 2 continued.

macaques (Table 1). In this study, we found a repeat number polymorphism in the A stretch in intron 2 in both *ULBP2.1* and *ULBP2.2* from both rhesus and cynomolgus macaques. Polymorphisms in exons 2 and 3 and intron 2 including the repeat polymorphism were included in the allele designation. Nucleotide sequences of *Mamu-ULBP2.2*1* and *Mafa-ULBP2.2*1* were identical to those of LOC694600. That the identical *ULBP2* alleles were shared in part by both rhesus and cynomolgus macaques was consistent with a cross-breeding between these macaques as suggested by the studies of diversity in the MHC class I genes (Saito et al. 2012).

Divergence of *ULBP2* genes in the higher primates

Nucleotide sequence homologies among the alleles of *ULBP2.1* and *ULBP2.2* in rhesus and cynomolgus macaques were 94.3 and 98.7 %, respectively, suggesting that *ULBP2.2* is less diverged than *ULBP2.1*. To figure out the evolutional divergence and diversity of *ULBP2* genes in the higher primates, we conducted a neighbor-joining analysis by using nucleotide sequences of exons 2 and 3 from *ULBP2.1* and *ULBP2.2* in macaques along with sequences of corresponding region from *ULBP2* and/or *ULBP6* reported for human, chimpanzee, gorilla, and another Old World monkey, olive baboon. *ULBP5* sequences from human and rhesus were also included in the analysis. As shown in Fig. 1, alleles of *ULBP2.1* and those of *ULBP2.2* in macaques were separately clustered, but both rhesus and cynomolgus alleles were found in the same cluster. Quite interestingly, *ULBP2.2* of macaques including olive baboon *ULBP2* and rhesus *ULBP5* appeared to be diverged from an ancestral *ULBP2.1*. In addition, *ULBP2* sequences from human, gorilla and chimpanzee as well as *ULBP5* and *ULBP6* sequences from human were clustered as a branch of *ULBP2.1* (Fig. 1). Furthermore, when other *ULBP* genes, *ULBP1*, *ULBP3*, and *ULBP4*, were included in the phylogenetic analysis, these genes were also clustered as

another branch of *ULBP2.1*, implying that these genes were diverged from the ancestral *ULBP2* in the primates (Supplementary Figure S1).

Diversity of *ULBP2* genes in the Old World Monkey

As for the diversity of *ULBP2* in macaques, non-synonymous substitutions were found at 14 sites in *Mamu-ULBP2.1*, 10 sites in *Mafa-ULBP2.1*, 15 sites in *Mamu-ULBP2.2*, and 16 sites in *Mafa-ULBP2.2* (Table 2). Amino acid sequences were deduced from the nucleotide sequences and alignment of the ULBP2 alleles showed that the ULBP2/RAET1H molecules in rhesus and cynomolgus macaques were homologous by more than 90 % to the human ULBP2 molecule in the α1 and α2 domains (Fig. 2). Among the polymorphic amino acid residues, six and eight residues in the ULBP2.1 and ULBP2.2 molecules, respectively, were observed in both rhesus and cynomolgus macaques (Fig. 2).

To investigate a possible role of the polymorphic residues, we created 3D structure models for ULBP2 molecules by referring the crystallographic data for human ULBP3 in complex with NKG2D, where ULBP2 residues at positions 22, 23, 70, 73, 77, 80, 83, 94, 165, 169, 170, and 172 composed of interacting surface with NKG2D (Supplementary Figure S2). It was found that three polymorphic residues at positions 73, 177, and 181 of rhesus ULBP2.1 were on the upper surface of α helix structures and pointed to the NKG2D receptor (Fig. 3a). Interestingly, the residue at position 73 could be a contacts site with Ser195 of NKG2D receptor, as deduced from the equivalent structure of human ULBP3. In contrast, none of the polymorphic residues were mapped on the surface of α helix structures in cynomolgus ULBP2.1 (Supplementary Figure S3).

On the other hand, two polymorphic residues at positions 158 and 181 of cynomolgus ULBP2.2 were on the upper surface of the α helix structure, while another polymorphic residue at position 172 was a possible interface site with Glu183 and Met184 of NKG2D in the equivalent human ULBP3, although it was not pointed up on the α helix of ULBP (Fig. 3b). In clear contrast and quite interestingly, none of the polymorphic residues were mapped on the surface of α helix in rhesus ULBP2.2 (Supplementary Figure S4). It should be noted here that the residue at position 20 is polymorphic in human ULBP2, while the residues at positions 80 and 172 are polymorphic in human ULBP6, indicating that both ULBP2 and ULBP6 might carry the allelic differences in the interaction with NKG2D in humans (Supplementary Figure S5).

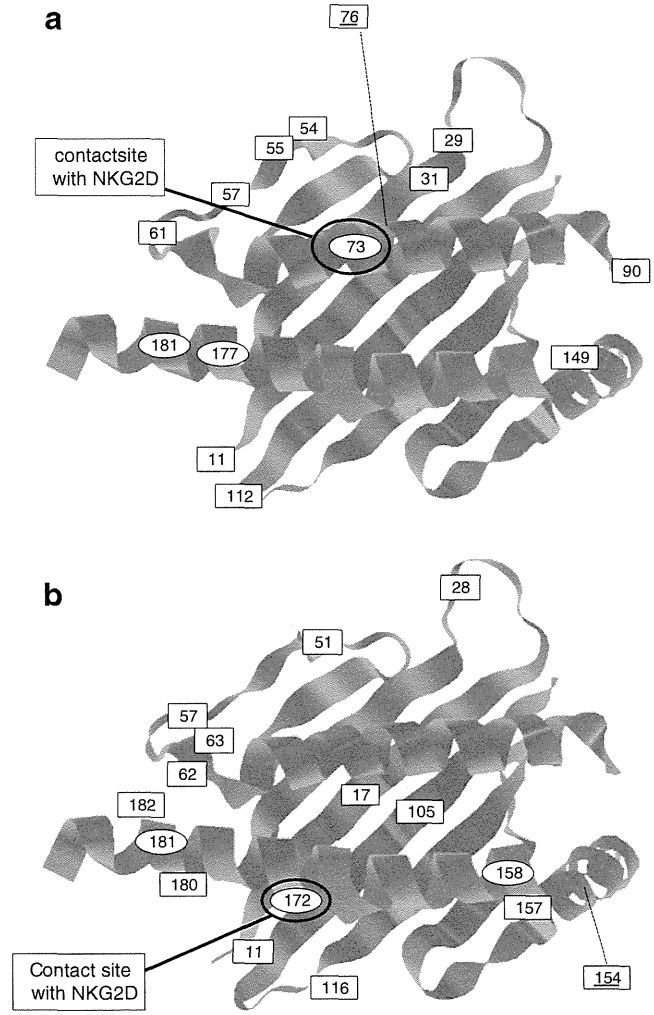

Fig. 3 Mapping of polymorphic sites on the 3D-structure model of macaque ULBP2 molecule. Polymorphic sites were mapped on the 3D structure model of ULBP2/RAET1H. Positions of polymorphic amino acid resides in the rhesus ULBP2.1 molecule (**a**) and cynomolgus ULBP2.2 molecule (**b**). Residues on the upper side of α helix are indicated by *circles*, while those on the outer side or on the β seat are indicated by *squares*. The residues mapped behind or beneath the α helix are underlined and represented by *dotted lines*. Possible contact sites with NKG2D (Radaev et al. 2001) are indicated

Discussion

In this study, we investigated the polymorphic nature of *ULBP2/RAET1H* in the Old World monkey. We previously reported that each member of the *ULBP/RAET1* gene family, except for *ULBP6/RAET1L*, was duplicated in the rhesus genome (Naruse et al., 2011). As expected, we obtained *ULBP2.1* and *ULBP2.2* sequences from both rhesus and cynomolgus macaques. On the other hand, any orthologous genes to human *ULBP6* were not detected in the macaques, even though *ULBP6* showed 96 % homology to *ULBP2* in humans (Radosavljevic et al. 2001). It was considered that *ULBP2.1* or *ULBP2.2* might be orthologous to human *ULBP6*. However, our phylogenetic analysis indicated that both human *ULBP2* and *ULBP6* were clustered with *ULBP2*s from chimpanzee and gorilla, as a branch of *ULBP2.1*. In addition, intron 2 sequences of ULBP2.2 in

macaques were relatively well conserved among *ULBP2*s from olive baboon, chimpanzee, western gorilla, and human as well as in human *ULBP6* than exon sequences. Furthermore, a Blast search showed that there was no *ULBP6*-like sequence in the genomes of chimpanzee and gorilla. These observations suggested that human *ULBP2* and *ULBP6* were diverged from an ancestral *ULBP2* after the diversification of human and other higher primates. The phylogenetic analysis also indicated that *ULBP2.2* might be diverged from *ULBP2.1* and the clustering of *ULBP2.1* alleles and *ULBP2.2* alleles did not depend on the species, supporting a trans-species evolution. Our observations were consistent with that ULBP/REAT molecule of placental mammals was originally diverged and duplicated in each species after an emigration from the *MHC* region (Kondo et al. 2010).

On the other hand, *Mafa-ULBP2.1*5* was placed at the diverging point of *ULBP2.2* in the phylogenetic tree (Fig. 1 and Supplementary Figure S1). As shown in Fig. 2, among the *ULBP2.1* alleles, only the *Mafa-ULBP2.1*5* has a replacement of Arg with Val at the position 105, which is a common feature of *Mamu-ULBP2.2* and *Mafa-ULBP2.2*. In addition, *Mafa-ULBP2.1*5* carries *ULBP2.2*-like sequences at the positions of 29 and 54. These characteristic features may eventually position the *Mafa-ULBP2.1*5* at the diverging point of *ULBP2.2*. Alternatively, gene conversion-like events from *ULBP2.2* had occurred in *ULBP2.1* to generate the *Mafa-ULBP2.1*5*.

In the present study, we denoted 15 and 11 *ULBP2.1* alleles and 11 and 10 *ULBP2.2* alleles in rhesus and cynomolgus macaques, respectively, of which more than 70 % of polymorphisms were non-synonymous. Induced expression of human ULBP2 molecule is involved in the recognition of virus-infected cell by NKG2D (Ward et al. 2009), although the functional significance of the polymorphisms in the extracellular domain of ULBP2 molecules remains to be deciphered. We demonstrated that several polymorphisms of ULBP2 molecules were located at the presumed contact sites with NKG2D or on the upper surface of α helix, which might have functional impacts. On the other hand, it has been reported that the sequence identities are less than 60 % among the ULBP molecules, while those between the ULBP and MIC molecules are about 25 % (Cosman et al. 2001). The interface residues appeared to be less conserved than the overall sequence among the ULBP molecules, and it was predicted that NKG2D could recognize the diversities of ULBP1 and ULBP2 molecules through induced-fit mechanisms in a similar manner as that of ULBP3 (Radaev et al. 2001). However, other previous studies revealed that the structural differences among the α2 domains of ULBP and MIC molecules affect the binding affinity to NKG2D and UL16, respectively (Wittenbrink et al. 2009; Spreu et al. 2006), suggesting that the ULBP polymorphisms demonstrated in this study might influence the efficacy of recognition by NKG2D. The functional impact of the polymorphisms should be investigated in future studies to decipher the evolutional and biological significance of the ULBP2 polymorphisms in the Old World monkeys.

Acknowledgments We thank Yukiko Ueda, Yasuko Saida, and Nana Ohkubo for their technical assistances. This work was supported in part by research grants from the Ministry of Health, Labor and Welfare, Japan and a Grant-in-Aid for scientific research from the Ministry of Education, Culture, Sports, Science, and Technology (MEXT), Japan. This work was also supported by a supporting program for women researchers from the Tokyo Medical and Dental University.

References

Antoun A, Jobson S, Cook M, O'Callaghan CA, Moss P, Briggs DC (2010) Single nucleotide polymorphism analysis of the NKG2D ligand cluster on the long arm of chromosome 6: extensive polymorphisms and evidence of diversity between human populations. Hum Immunol 71:610–620

Bacon L, Eagle RA, Meyer M, Easom N, Young NT, Trowsdale J (2004) Two human ULBP/RAET1 molecules with transmembrane region are ligands for NKG2D. J Immunol 173:1078–1084

Bauer S, Groh V, Wu J, Steinle A, Phillips JH, Lanier LL, Spies T (1999) Activation of NK cells and T cells by NKG2D, a receptor for stress-inducible MICA. Science 285:727–729

Chalupny NJ, Sutherland CL, Lawrence WA, Rein-Weston A, Cosman D (2003) ULBP 4 is a novel ligand for human NKG2D. Biochem Biophys Res Commun 305:129–135

Cosman D, Mullberg J, Sutherland CL, Chin W, Armitage R, Fanslow R, Kubin M, Chalupny NJ (2001) ULBPs, novel MHC class I-related molecules, bind to CMV glycoprotein UL16 and stimulate NK cytotoxicity through the NKG2D receptor. Immunity 14:123–133

Eagle RA, Traherne JA, Ashiru O, Wills MR, Trowsdale J (2006) Regulation of NKG2D ligand gene expression. Hum Immunol 67: 1159–1169

Eagle RA, Flack G, Warford A, Martinez-Borra J, Jafferji I, Traherne JA, Ohashi M, Boyle LH, Barrow AD, Caillat-Zucman S, Young NT, Trowsdale J (2009a) Celllar expression, trafficking, and function of two isoforms of human ULBP5/RAET1G. PLoS ONE 4:e4503

Eagle RA, Traherne JA, Hair JR, Jafferji I, Trowsdale J (2009b) ULBP6/RAET1L is an additional human NKG2D ligand. Eur J Immunol 39: 3207–3216

Gibbs RA, Rogers J, Katze MG et al (2007) Evolutionary and biomedical insights from the rhesus macaque genome. Science 316:222–234

Kondo M, Maruoka T, Otsuka N, Kasamatsu J, Fugo K, Hanzawa N, Kasahara M (2010) Comparative genomic analysis of mammalian NKG2D ligand family genes provides insights into their origin and evolution. Immunogenetics 62:441–450

Kulski JK, Anzai T, Shiina T, Inoko H (2004) Rhesus macaque class I duplicon structures, organization, and evolution within the alpha block of the major histocompatibility complex. Mol Biol Evol 21: 2079–2091

Matusali G, Tchigjou HK, Pontrelli G, Bernardi S, D'Ettorre G, Vullo V, Buonomini AR, Andreoni M, Santoni A, Cerboni C, Doria M (2013) Soluble ligands for the NKG2D receptor are released during HIV-1 infection and impair NKG2D expression and cytotoxicity of NK cells. FASEB J 27:2440–2450

Naruse TK, Chen Z, Yanagida R, Yamashita T, Saito Y, Mori K, Akari H, Yasutomi Y, Miyazawa M, Matano T, Kimura A (2010) Diversity of MHC class I genes in Burmese-origin rhesus macaque. Immunogenetics 62:601–611